applied nano

MDPI

Article

Application of Reduced Graphene Oxide-Zinc Oxide Nanocomposite in the Removal of Pb(II) and Cd(II) Contaminated Wastewater

Moeng Geluk Motitswe [1], Kassim Olasunkanmi Badmus [2,*] and Lindiwe Khotseng [1]

[1] Chemistry Department, University of the Western Cape, Cape Town 7535, South Africa; moeng.geluk@gmail.com (M.G.M.); lkhotseng@uwc.ac.za (L.K.)
[2] Industrial Chemistry Department, First Technical University, Ibadan 23401, Nigeria
* Correspondence: kassim.badmus@tech-u.edu.ng

Abstract: Toxic metal wastewater is a challenge for exposed terrestrial and aquatic environments, as well as the recyclability of the water, prompting inputs for the development of promising treatment methods. Consequently, the rGO/ZnONP nanocomposite was synthesized at room temperature for four hours and was tested for the adsorption of cadmium and lead in wastewater. The optimized nanocomposite had the lowest band gap energy (2.69 eV), and functional group interactions were at 516, 1220, 1732, 3009, and 3460 cm^{-1}. The nanocomposite showed good ZnO nanoparticle size distribution and separation on rGO surfaces. The nanocomposite's D and G band intensities were almost the same, constituting the ZnO presence on rGO from the Raman spectrum. The adsorption equilibrium time for cadmium and lead was reached within 10 and 90 min with efficiencies of ~100%. Sips and Freundlich best fitted the cadmium and lead adsorption data (R^2 ~ 1); therefore, the adsorption was a multilayer coverage for lead and a mixture of heterogenous and homogenous coverage for cadmium adsorption. Both adsorptions were best fitted by the pseudo-first-order model, suggesting the multilayer coverage dominance. The adsorbent was reused for three and seven times for cadmium and lead. The nanocomposite showed selectivity towards lead (95%) and cadmium (100%) in the interfering wastewater matrix. Conclusively, the nanocomposite may be embedded within upcoming lab-scale treatment plants, which could lead to further upscaling and it serving as an industrial wastewater treatment material.

Keywords: toxic metal; cadmium; lead; wastewater; nanocomposite; adsorption; Sips; Freundlich; pseudo first order

Citation: Motitswe, M.G.; Badmus, K.O.; Khotseng, L. Application of Reduced Graphene Oxide-Zinc Oxide Nanocomposite in the Removal of Pb(II) and Cd(II) Contaminated Wastewater. *Appl. Nano* **2024**, *5*, 162–189. https://doi.org/10.3390/applnano5030012

Academic Editors: Sara Cerra and Ilaria Fratoddi

Received: 19 June 2024
Revised: 7 August 2024
Accepted: 9 August 2024
Published: 9 September 2024

1. Wastewater

Clean and portable water plays an essential role in the preservation and maintenance of livelihoods in aquatic and terrestrial habitats. Nevertheless, there is the ongoing problem of clean water provision at an adequate rate relative to the growing human population demand, which in turn promotes industrialization-based effluents to the air, soils, and available surface and groundwater resources, resulting in water pollution. Wastewater may contain chemical, physical, and biological pollutants. Amongst these contaminants, toxic metals are regarded to be highly resistant to conventional treatment due to their solubility and non-biodegradability in water, and, as a result, they contribute secondary pollution, thus leading to the non-suitability of the treated wastewater for human and animal consumption. The metals are mostly sourced from industrial works such as manufacturing, paper, pharmaceutical, smelting, and mining operations. Consequently, the toxic metal wastewater generation may lead to clean water supply challenges, scarcity, and expense to affected communities. Additionally, the inert nature of toxic metals may influence their environmental persistence and bioaccumulation, as well as bio magnification. Toxic metals are undoubtedly a potential health hazard [1]. The risks to human and

environmental as a result of the presence of toxic metals are enormous [2]. Designing and synthesizing nanocomposites as adsorbents for the effective removal of toxic metal from wastewater is highly desirable, likewise is the application of a cost-effective raw material such as graphene [3]. The significance of graphene-based nanocomposites includes its possession of excellent mechanical, thermal, electrical, and chemical properties [4]. These materials can be applied as adsorbents to ensure the complete elimination of toxic metals from aqueous systems. The enhancement of surface area and multiple functional groups in graphene-based adsorbents leads to their superior toxic metal adsorption potential [5].

1.1. Impact of Toxic Metal Presence in Wastewater and Challenges of Their Removal

Although metal abundance has been naturally experienced on Earth for several years since approximately 75% of the gross elements in the chemical periodic table are ranked as metals, most of the environmental depositions are sourced from daily anthropogenic activities (industrial production, smelting, mining operations, agricultural, batteries, and galvanizing works) [6]. Consequently, toxic metals participate in most of the trace inorganic contaminants as outlined by the US Environmental Protection Agency [7]. Toxic metals are explained to be elements with a density greater than 5 g/cm^3 that have a high atomic mass, as well as having persistence, pose toxicity to the water source, and, thus, cause wastewater. Moreover, toxic metal water contamination may also occur via sediment resuspension, metal ion soil erosion, leaching, atmospheric discharge, and metal from water resources to groundwater [6]. Among all the pollutants, toxic metals participate in the pollutant pool, and most of them are readily soluble in water, especially in sulphate and nitrate forms, thus posing a challenge in wastewater treatment due to their long life span, ability to form oxidative species, and persistence in the environment. Unfortunately, toxic metals tend to accumulate without being seen in the host environment, unlike the municipal waste and petroleum hydrocarbons, thus placing the challenge in the remediation process, which may result in the consumption of polluted water for use in house, agricultural, and industrial applications with subsequent health and production impairments.

1.1.1. Lead (Pb)

Lead is described as an element with greater density and atomic mass in comparison to water molecules. In fact, lead possesses a density of 11.34 g/cm^3 and a weight of 207.2 g/mol; thus, it is considered to be one of the heavy metals in water. Lead has been used in several industrial applications such as plumbing, explosives, batteries, gasoline, and cosmetic manufacturing. Gradual lead intake through drinkable water can cause abdominal cramps, diarrhea, vomiting, nausea, reproductive, renal, central nervous system malfunctions, depreciated seedling growth, abnormal root length, mitosis cell division and photosynthesis in humans, animals, and plants [8,9]. In patients, unmonitored iron intake may destructively damage the gastrointestinal mucosa and hypovolemia sourced from blood loss too. These could result in the mortality of affected patients (humans and animals) [10]. Consequently, the elimination of lead ions in drinkable water and wastewater is essential for adequate water and source conservation.

1.1.2. Cadmium (Cd)

Cadmium is an element with a density of 8.65 g/cm^3 and an atomic mass of 112.41 g/mol greater than water. Its uses include anti-corrosion electroplating, plastic stabilization, batteries, pigmentations, and solar cells. On the other hand, the unmonitored accumulation of cadmium and its compounds renders cadmium a toxic element prevalent in the industry that discharges effluents that get into the waterways, resulting in environmental pollution, human, and animal wellbeing defects. Consequently, the use of cadmium is decreasing due to its toxicity trait. The International Agency for Research on Cancer and the National Toxicology Program has declared cadmium as a carcinogen (prostate, lung, urinary, kidney, and breast cancer) in humans and animals [11]. Additionally, the carcinogenicity mechanism is reported to be multifactorial. Cadmium toxicity causes water

and nutrient translocation, and metabolism and photosynthetic disruptions, and uplifts reactive oxygen species generation, which initiates both the cell biomolecule destruction and plant membrane damage [12]. Commonly, cadmium may destruct the uptake and mass transport of nutritional elements such as magnesium, calcium, and potassium in plants. Conclusively, this constitutes the essentiality of cadmium removal in wastewater for safer use for residential, industrial, and agricultural purposes.

1.2. Cadmium and Lead Wastewater Treatment

Toxic metal emissions and related effluents are regarded as prominent health challenges to both terrestrial and aquatic organism and their habitats. Several traditional methods such as chemical precipitation, ion exchange, solvent extraction, coagulation, and flocculation have been explored for use in metal treatment. Among the aforementioned techniques, the adsorption method offers a variety of applications in comparison to other methods relative to their drawbacks, for example, the large production of sludge, expensive disposal, low efficiency, and sensitive operating conditions [13]. Although they have a track record of removing the metals, adsorption is more practical, efficient, and feasible due to its operation simplicity, design simplicity, ability to remove contaminant concentration under 100 ppm, unlike other methods, less or no sludge generation, and environmental friendliness. It also fairly supports recycling and reusing applications [14]. The adsorption method is a method that includes the deposition of gas or liquid (adsorbate) on a solid surface (adsorbent), resulting in molecular film formation.

The process is partitioned into two types, which are chemisorption and physisorption. Chemisorption is described to be adsorption through chemical bonding (which includes the generation of covalent or ionic bonds via chemical reactions), whereas physisorption occurs through physical interaction between the adsorbent and adsorbate and is considered non-specific since it supports random and multilayer adsorption. As a result, precipitation, redox reactions, simplified diffusion, hydrogen bonding, complexation, and electrostatic interaction are feasible mechanisms to adsorb toxic metal ions onto the adsorbent surface for water treatment.

Furthermore, the adsorption method may be monitored by variations in process parameters such as pH, temperature, contact time, and initial concentration [15]. Additionally, the process's efficiency is also attributed to the adsorbent's nature—active sites/surface area, kinetics, and selectivity [16]. As a result, several toxic metals including Cd and Pb have been successfully removed via adsorption with high adsorption amounts, capacity, and removal efficiencies [17,18]. Moreover, the regulated maximum contaminant or permissible limits assigned by the World Health Organization for Cr (chromium), Ni (nickel), Pb (lead), Cd (cadmium), As (arsenic), Cu (copper), Hg (mercury), zinc (Zn), and cobalt (Co) in drinkable water are 0.05, 2.0, 0.05, 0.003, 0.01, 2.5, 0.001, 5.0, and 0.1 mg/L, and there is a need for monitoring and treating their amounts in water and wastewater [19].

1.2.1. Nanotechnology and Nanomaterials

Nanotechnology is defined as technology at the nanoscale level in which systems, devices, or materials are fabricated through controlling the matter at the nanoscale length to enhance unique material properties at the nano-level [20]. Moreover, nanotechnology includes several nanomaterials—described as materials having at least one dimension in the nanoscale range of 1–100 nanometers (nm). Their versatility allows them to be applied not only in wastewater treatment but also in sensors, pharmaceuticals, and electronics. In contrast to conventional materials, nanomaterials have an improved surface area, catalytic activity, porosity, shape, lighter weight, electrical properties, high reactivity, adsorption, and catalytic nature [21]. These materials and associated synthesis techniques, removal principles, and application routes have shown a promising affinity towards toxic metal removal in wastewater as compared to the bulk conventional adsorbents [22].

1.2.2. Reduced Graphene Oxide/Metal Oxide (rGO/MO) Nanocomposite

Multiple studied adsorptive materials capable of removing metals from aqueous solutions are clays, biological and agricultural waste, fly ash, chitosans, zeolites, natural oxides, peat moss and activated carbon [23–26]. However, the reported limitations of these adsorbents are their relatively small metal-binding constants, small selectivity, low removal capacities, instability at low or high pH values, and intolerance for high toxic metal ion concentrations [27,28]. The current manuscript will be setup as presented as presented in Figure 1.

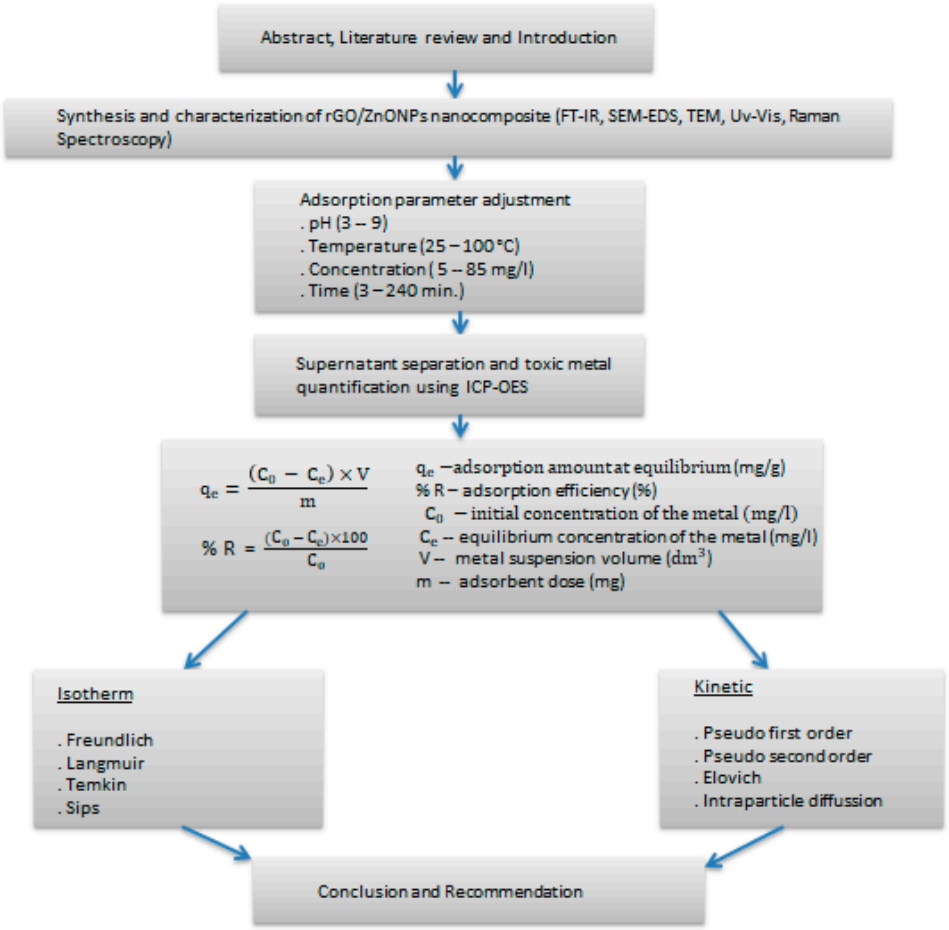

Figure 1. Research roadmap in the current study.

2. Review

2.1. Challenges with Various Nanoparticles for the Treatment of Toxic Metals

Recent research projects have shown that metal oxide nanoparticles exhibit capabilities for toxic metal ion removal in wastewater [29,30]. Nanotechnology has gained prominent interest in the environmental application field due to its associated controllable physicochemical properties, magnetism, and larger surface area [31]. However, the common challenge with toxic metal removal application has been separation or instability in agglomeration [32,33]. It has been evidenced that the single metal nanoparticles suffer good separation after wastewater treatment, thus, gradually combatting their recycle and reuse phase. This could cause the generation of secondary pollutants, and, if they are treated by biological and photocatalytic adsorbent regeneration, these methods could be unsuitable and unsafe for treating spent adsorbent since the methods rely on contaminant degradation and combustion [34,35].

However, among the various materials used for toxic metal water treatment, metal oxide nanoparticles such as cerium oxide (CeO_2), iron oxide (Fe_3O_4 and Fe_2O_3), titanium oxide (TiO_2), and zinc oxide (ZnO) exhibit improved tunable functionalization, surface

reactivity, selectivity, and photocatalytic nature. They also act as exceptional adsorbents for wastewater remediation due to their affinitive surface functional groups towards various toxic metals including Pb (II) and Cd (II) [36–39]. Among the metal nanoparticles, zinc oxide nanoparticles have received pronounced attention for wastewater treatment since their material may act as a precipitant, photocatalytic, and adsorbent agent for selected toxic metals [40–43]. The possible property drawbacks associated with ZnO nanoparticles are agglomeration, instability, leaching, and depreciated thermal characteristics for efficient application during toxic metal uptake in wastewater [44–46]. Therefore, the synthesis of surfacing the nanoparticles onto the supporting material with a high surface area has been a feasible, with ongoing research interest resulting in good nanocomposite material; thus, it was investigated in this study.

2.2. Nanocomposite

The graphene material has drawn attention due to its leading optical, mechanical, thermal, and flexibility properties [47]. Reduced graphene oxide as a graphene derivative is majorly synthesized by the generation of graphite oxidation to graphene oxide and the reduction of oxygen content on the graphene sheets by thermal and chemical treatment leading to multifunctional surface generation [48]. The functionalizable surface of the reduced graphene oxide allows for the impregnation of the nanoparticle materials on the graphene layers to produce a smooth sorption surface [49]. Moreover, the material may be in macro clusters while the sorption surface may become regular. Although there are some limitations with chemical modification, this method gives a control on tuning the functional groups for subsequent improved adsorption efficiency and selectivity for wastewater treatment [49,50].

Reduced graphene oxide/metal oxide nanocomposites have been synthesized in various ways aiming at achieving chemical (advanced chemical stability), physical (high thermal and electrical conductivity, mechanical strength, large surface-to-volume ratio, porosity, and capacitance) and biological (antiviral, antibacterial, and antioxidant) properties, which serve as promising and compatible characteristics for supercapacitors, fuel and solar cells, drug delivery, tissue engineering, cancer treatment, and biosensors [51–53]. The graphene/ZnO electrochemical sensor for para-nitrophenol was successfully developed and recorded a low detection limit of 8.8×10^{-9} M using square wave voltammetry [54]. The sensor proved to exhibit high sensitivity and specificity for para-nitrophenol against interfering compounds, which are ortho-nitrophenol, 2,4-di-nitrophenol, and meta-nitrophenol, in groundwater and river samples. These also signify that the composite resulted in an improvement of the electrochemical performance of the modified glassy carbon electrode, which led to improved and fast recoveries [54]. In another study, the graphene/ZnO nanocomposite was tested for a supercapacitor project where the material performed well with 122.4 F/g in comparison to rGO (102.5 F/g) and graphene oxide (2.13 F/g) [55]. The good performance was attributed to the well-dispersed electronegative ZnO particle (with a size between 30 and 70 nm, which qualifies the large surface area and high electron mobility) on the graphene sheet and the synergistic effect sourced between the nanocomposite structure, which was confirmed by EDS, HRTEM, XRD, UV–vis and galvanostatic charge/discharge techniques, and cyclic voltammetry, thus resulting in a potential electromaterial for an advanced supercapacitor purpose. The graphene/ZnONP nanocomposite exhibits a good carriage and pH-sensitive ejection of conjugated and aromatic anticancer drugs [56]. Furthermore, the composite possesses the capability for endosomal escape post intracellular use for genetic therapy and transportation; hence, the material is a promising candidate for cancer therapeutics, drug delivery, and co-delivery [56–58].

ZnO is considered as a wide band-gap semiconductive material consisting of a large charge carrier recombination leading to its possible instability and decreased photocatalytic efficiency [58]. In order to accommodate the drawbacks, the material has been modified with other metal oxides, polymers, zeolites, and nanocarbon-based materials for photocatalytic behavior improvement [58].

Importantly, the graphene material has proved to efficiently hybridize with ZnO for catalytic characteristics. The zinc oxide nanorods were hydrothermally deposited on bilayered reduced graphene oxide for the photodegradation of methyl orange in water. The degradation efficiency increased by 15% when the composite was tested as compared to the unmodified zinc oxide nanorods. Furthermore, the composite reaction rate (1.4×10^{-2} min^{-1}) was higher than the rGO (1×10^{-3} min^{-1}) and ZnO (7.2×10^{-3} min^{-1}), proving a fast kinetic reaction due to the synergistic interactions sourced from the composite's rGO and ZnO [59]. In another study, the rGO/ZnO nanocomposite was applied in gas to liquid conversion through the photoreduction of carbon dioxide (CO_2) to methanol (CH_3OH). The CH_3OH yields for rGO/ZnO nanocomposite and ZnO nanorods were 263.17 and 52.36 $\mu mol/g_{cat}$ [60]. This indicated the five times increase in CH_3OH yield from a pure ZnO to rGO/ZnO nanocomposite, which could be sourced from an improved charge separation and catalytic activity by a nanocomposite photocatalyst. Furthermore, the nanocomposite proved to support the improved photoreductive stability, cycling, and reusability properties with a minimal decrease of 5% in the CH_3OH yield [60].

As a result, these cases serve as proof of graphene/ZnONP nanocomposites being multifunctional materials that are compatible with various applications. Therefore, the current study is aligned with water treatment, and the review will majorly be on toxic metal removal from wastewater using the selected nanocomposite through the adsorption method.

Recently, to overcome these limitations, nanolayered rGO (reduced graphene oxide) functionalized with MO (metal oxide) nanoparticles allowed for available adsorbate binding sites, with improved selectivity, surface area, and adsorption capacities, as well as no/less particle–particle aggregation. Further efficiencies have been studied for wastewater treatment [61,62]. A study recorded the high adsorption capacities and efficiencies of selected metals in the range of 100–600 mg/g, and greater efficiencies than 85% have been obtained with rGO/ZnONP nanocomposites [19,63,64]. Several studies have been conducted on cadmium and lead removal using GO/ZnONP composites as compared to rGO/ZnONP nanocomposites [65–68]. As a result, this study focuses on rGO/ZnONP nanocomposite synthesis and adsorptive application in the remediation of cadmium and lead in wastewater.

2.3. Adsorption Limitations

Although adsorption is regarded as a simple and efficient method for toxic metal treatment, the generation of suitable adsorbing materials may not be cost-effective, and some adsorbents like commercialized activated carbons may not allow for recycling post the water treatment (Table 1). This could lead to potential unsustainable large-scale toxic metal wastewater remediation [19,69]. As a result, the drawbacks may be fairly accommodated with moderate to low-cost, recyclable, and reusable nanocomposite adsorbent, which outputs efficient metal uptake. In this context, this study investigated the fabrication of rGO/ZnONP nanocomposite as a promising adsorbent for uptaking Cd and Pb with the aid of reuse, and interfering species, and monitoring the adsorption through various process parameters, equilibriums, and kinetic models.

2.4. rGO/ZnONP Nanocomposite for Treatment of Pb and Cd in Wastewater

2.4.1. Cadmium (Cd) Wastewater Treatment

The zinc oxide nanoparticles were prepared by co-precipitation. The achieved nanoparticles were confirmed by XRD to have a hexagonal phase structure. Furthermore, the graphene oxide layers were fabricated via the Hummers method, and the Aloe vera leaf extract was used for the conversion of graphene oxide to reduced graphene oxide [70]. Although the ZnO nanoparticles seemed to have swallowed the graphene material peak, the overall composite's crystallinity, surface functionalization, and morphology were evidenced by XRD, TEM, and AFM. The composite's average crystallite size was 70 nm, with the surface wrinkled and roughness showing the composite generation. The uptake of the

cadmium by the ZnO/rGO was investigated based on time (0–120 min) and pH (2–8). The results showed that the adsorption efficiency increased relative to the pH increase, and this could be due to competition for available and reactive sites for H^+ and Cd^{2+} adsorption. Although the removal efficiency increases, the Cd at pH 8 could form a precipitate that depreciates the adsorption and possible desorption for reuse. Therefore, pH 6 was preferred with efficiency greater than 80% [70]. The sonochemical method was used for the PANI/ZnO/r-GO synthesis, which was found to be an amorphous, semi-agglomerated surface [67]. The material was applied for Cd adsorption, which was optimally achieved at the time (60 min: 60.9%), adsorbent quantity (0.2 g: 63%), temperature (60 °C: 57%), pH (6: 98%), and concentration (10 mg/L: 24%). The adsorption was well described by Freundlich (R^2 = 0.99) and pseudo second order (R^2 = 0.95) as compared to Langmuir (R^2 = 0.93), Jonavoic (R^2 = 0.97), and pseudo first order (R^2 = 0.94). This implied that the adsorption was a non-specific uptake and proceeded through multi-layered configuration [67]. In conclusion, multiple studies have been conducted on the effect of ZnO/rGO composites for Cd removal with uplifted efficiencies [66,71,72].

2.4.2. Lead (Pb) Wastewater Treatment

In another study, the ZnO/rGO nanocomposite was sono-chemically synthesized for Pb (II) adsorption. The composite was found to be semi-crystalline, photoactive, sphere-shaped nanoparticles dispersed on rGO sheets with some agglomeration [73]. The adsorption process was optimized pH (2–6), contact time (0–70 min), concentration (20–100 mg/L), temperature (5–80 °C), and adsorbent dosage (20–100 mg). The optimum parameters were 60 min, 100 mg, pH 6, 20 mg/L, and 65 °C with maximum removal efficiencies of 68, 68, 98, 17, and 57%, respectively. The adsorption data well fitted Langmuir isotherm and pseudo first order with the highest regression coefficients of 0.993 and 0.973. The composite sustained three recycling phases (with 0.1M HCl) for reuse with the following descending efficiencies: 78, 63, and 41% [73]. The removal deficiency could have been due to unsuccessful full desorption and significant surface compositional change when exposed to the Pb as evidenced by the presence of irregular agglomerates as shown in the SEM images after the adsorption [73]. The ZnO/rGO nanocomposite was hydrothermally synthesized in an autoclaved reactor at 180 °C for 6 h [71]. The nanoparticle's TEM image showed spherical shapes deposited on the graphene sheet. The adsorption of Pb (II) was then investigated from 1 to 50 mg/L (initial concentration), 10 to 50 mg (adsorbent quantity), and the maximum capacity was achieved under room temperature for five minutes. As a result, 50 mg of the adsorbent dose, pH 6, resulted in the highest removal efficiency of 75.4%. The adsorption improvement by functionalizing the graphene's surface with ZnO nanoparticles has been evidenced in other studies too [68,74,75].

Table 1. Adsorption of Pb (II) and Cd (II) in wastewater using graphene-oxide-based composite materials.

Adsorbent	Adsorbent Nature	Equilibrium Time (min)	Toxic Metal Treated	Adsorption Efficiency (%)	Kinetic and Thermodynamic Model	Recycle Reaction	Refs.
$ZnFe_2O_4$/rGO	Crystalline, rough and wrinkled surface, and weak magnetism	60	Pb (II)	98	Langmuir and pseudo second order (chemisorption)	5	[76]
ZnO/GO	Weak crystallinity, hollow-shaped spaces, and flake-shaped morphology	120	Pb (II); Cd (II)	97; 96	Langmuir and pseudo second order (chemisorption)	-	[77]
ZnO/G	Well-surfaced spherical ZnO nanoparticles on graphene	25	Pb (II)	92	Endothermic, spontaneous, Langmuir, and pseudo second order	3	[75]

Table 1. *Cont.*

Adsorbent	Adsorbent Nature	Equilibrium Time (min)	Toxic Metal Treated	Adsorption Efficiency (%)	Kinetic and Thermodynamic Model	Recycle Reaction	Refs.
Fe_3O_4/rGO	Homogeneously dispersed nanoparticles on rGO sheet and magnetic and thermally stable composite	45	Pb (II)	96	Exothermic and spontaneous reaction, Temkin, chemisorption, and liquid film diffusion	-	[78]
CuO/rGO	Homogeneously dispersed nanoparticles on an rGO sheet with minimal sheet agglomeration	175	Cd (II)	91	Langmuir	-	[79]
TiO_2/rGO	Irregular and mesoporous surface	150	Pb (II)	89	Langmuir and pseudo second order	-	[80]
ZnO/rGO	Good distribution of ZnO nanoparticles on rGO sheet and wrinkled surface	90	Cd (II)	90	Langmuir, pseudo second order, and chemisorption	-	[70]
PTP-SiO_2/rGO	Sphere-shaped nanoparticles distributed moderately on rGO surface and amorphous nature	60	Cd (II), Pb (II)	62, 66	Jovanovic isotherm, spontaneous adsorption, and pseudo second order	3	[81]
WO_3/rGO	Increased average crystallite size upon surfacing on rGO, strong bonding existing between WO_3 and rGO, signaled by weakening and broadened WO_3 Raman spectroscopy peak, and mesoporous surface	200	Pb (II), Cd (II)	93.35, 89.95	Electrostatic attraction	-	[82]
FA/GO	Well-covered graphene oxide surface by folic acid with uplifted roughness and irregularly shaped composite surface	90	Cd (II)	82	Freundlich isotherm, pseudo second order, endothermic, multilayered, and spontaneous adsorption	2	[83]
Mn–Fe_3O_4/G	Weak magnetism and well-dispersed particle on a graphene sheet	58	Cd (II)	94	Langmuir–Redlich–Peterson isotherm, spontaneous removal, chemisorption, and pseudo first and pseudo second order	2	[84]
ZnO/rGO	Slight agglomerated surface, sheet-like structure, and electronegative and photo-active surface	10, 90	Cd (II), Pb (II)	~100	Freundlich, Sips, and pseudo first order	3, 7	This study

2.5. Experimental Procedure

2.5.1. Zinc Oxide Nanoparticles (ZnONPs)

A total of 0.5 M $ZnSO_4.7H_2O$ (100 mL) was precipitated with 1 M NaOH (100 mL) at room temperature for 3 h. The obtained white precipitate was washed with 0.5 M MeOH (250 mL) and 200 mL of deionized water. Lastly, the product was oven-dried at 100 °C for 35 min and calcined at 200 °C for 2 h.

2.5.2. Reduced Graphene Oxide (rGO)

H_2SO_4 (50 mL) was pre-cooled for 30 min in an ice bath. Thereafter, the graphite (3 g) and $NaNO_3$ (1.5 g) were added to H_2SO_4 (50 mL) with continuous stirring for 30 min in an ice bath. Moreover, $KMnO_4$ (3 g) was moderately added for an hour while stirring. Afterwards, the mixture was stirred at 40 °C and added to H_2O (100 mL). Furthermore, the composition was stirred for an additional 2 h at 90 °C and added to H_2O (50 mL) with H_2O_2 (6 mL) for an additional 2 h. Then, the graphene oxide (GO) was filtered and washed with H_2O (~500 mL) and 0.5 M MeOH (50 mL). The resultant black precipitate was dried at ~100 °C overnight.

For reduction, the dried GO (1 g) was dissolved into H_2O (100 mL) with $NaBH_4$ (0.2 g) for 4 h at 100 °C in a reflux setup, followed by bath ultrasonication (2 h) for sheet exfoliation. Lastly, the graphene was washed with H_2O (200 mL), dried at ~100 °C overnight, and thermally treated in the tube furnace at 350 °C (10 °C/min) for 2 h under nitrogen flow.

2.5.3. rGO/ZnONP Nanocomposite

A weight ratio of 1:3 (*w*/*w*) (rGO/ZnONPs) was used for composite synthesis. The rGO/ZnONP nanocomposite was prepared by the dispersion of reduced graphene oxide in ethanol (99%) and mixing with ZnONP powder while continuously stirring in an inert environment for 1 to 6 h. Thereafter, the resultant black–white precipitate was washed with 1 M ethanol (50 mL) and deionized water (100 mL) to remove excess solvent and dried in a vacuum oven at 100 °C for 30 min.

2.6. Characterization of Adsorbents

The adsorbent was analyzed for its material characteristics. FT-IR, UV–vis, TEM, and Raman spectroscopy were used to investigate the functional groups present, optical nature, surface morphology, elemental composition, and defect density in the adsorbent.

The functionalization was studied using attenuated total reflectance FT-IR from 400 to 4000 cm^{-1} in five replicate scans. A spectral resolution of 4 cm^{-1} using Perkin–Elmer-Spectrum100 FTIR spectrometer was used, coupled with universal ATR top plate and diamond crystal. Furthermore, UV–vis analysis was conducted by dissolving 0.0015 g of the synthesized material in 20 mL of deionized water and using a quartz cuvette of a light path of 1 cm. The UV–vis measurements were carried out on a Wirsam Scientific, Johannesburg, South Africa, (UV/vis 920) GBC instrument with the processing parameters as follows: step size (0.133 nm), speed (300 nm/min), slit width (2 nm), and results read by Cintral v 2.4 software. TEM imaging was obtained using FEI Tecnai G2 20 field-emission gun (FEG) TEM, employed in bright field mode at an accelerating voltage of 200 kV. The sample preparation was carried out by evenly dispersing fine-powdered samples over carbon tape attached to copper stubs. Thereafter, the samples were gold capped using the sputtering tool for clear scanning electron microscope observations. Raman spectra were conducted using the Jobin–Yvon LabRAM HR Raman spectrometer. X-ray diffraction (XRD) patterns were recorded in the range of $2\theta = 0°–90°$ using a Rigaku Miniflex X-ray powder diffractometer with Cu Kα radiation (λ = 1.5406 Å, operated at 40 kV and 40 mA).

3. Adsorption Study

Batch tests were performed to study the impacts of initial solution pH values, dosage, contact time, initial concentration, and temperature on the adsorption capacity of Pb (II) and Cd (II) ions using rGO/ZnONPs. Separately, 100 mL of Pb (II) and Cd (II) synthetic wastewater was prepared from $Pb(NO_3)_2.4H_2O$ and $CdC_4H_6O_4.2H_2O$ while magnetically stirring at 180 rpm with the adsorbent. After the equilibrium, the aqueous phase was separated from solids by centrifugation (3000 rpm, 15 min) and subsequently filtered through 0.22 µm membranes to quantify Pb (II) and Cd (II) residual concentration. The triplicate equilibrium concentrations of Pb (II) and Cd (II) were measured via the ICP-OES instrument. Moreover, the resultant adsorbent was exposed to desorption by using a 0.01 M H_2SO_4 (50 mL) solution for 45 min under magnetic stirring (80 rpm). This resulted in

adsorbent recycling and allowed for further reuse. Afterwards, the recycled rGO/ZnONPs were separated by centrifugation (3000 rpm for 15 min). The supernatant was then decanted and allowed to dry at 40 °C for 20 min before being employed for further metal adsorption.

The interference study was carried out by the one-pot method made up of copper, iron, chromium, zinc, cadmium, and lead. A total of 90 mg, pH 5, 25 °C, 10 ppm (for each metal), 200 rpm, and 4 h were applied during the testing.

The equilibrium removal capacity and efficiency were determined using Equations (1) and (2):

$$Q_e = \frac{(Co - Ce) \times V}{m} \quad (1)$$

$$\% \text{ R} = \frac{(Co - Ce) \times 100}{Co} \quad (2)$$

where V is the suspension volume (dm^3), m is the adsorbent weight (g), C_o is the initial concentration (mg/L), and C_e is the aqueous-phase equilibrium metal concentration (mg/L).

3.1. Adsorption Isotherms

The batch experimental data were fitted by using Langmuir, Freundlich, Tempkin, and Sips models in the determination of sorption capacity via Equations (3)–(6).

$$q = \frac{q_L K_l C_e}{1 + K_l C_e} \quad (3)$$

$$q = K_F C_e^{\frac{1}{n}} \quad (4)$$

$$q = \text{B } \ln A_t C_e \quad (5)$$

$$q = \frac{(q_m (K * C_e) \hat{} n)}{\left(1 + (K * C_e) \hat{} n\right)} \quad (6)$$

where

q = amount adsorbed (mg/g);
q_L = adsorption capacity related to a monolayer surface coverage;
K_l = Langmuir constant corresponding to the adsorption energy;
K_F = Freundlich constant related to the adsorption capacity;
A_t = equilibrium binding constant related to Tempkin isotherm;
n = adsorption intensity constant;
C_e = metallic equilibrium concentration in aqueous phase (mg/L);
B = abbreviation of RT/b_t, R—gas constant (8.314 J/mol K), and K—absolute temperature;
b_t = Tempkin isotherm constant;
q_m = maximum amount adsorbed;
K = Sips isotherm model constant.

3.2. Adsorption Kinetics

For the investigation of kinetics, 0.015 and 0.050 g of rGO/ZnONPs were added to 100 mL of Pb^{2+} solution (3 mg/L) and Cd^{2+} (10 mg/L). The suspensions were stirred at 180 rpm under room temperature. The samples were withdrawn at 3 to 240 min. Afterward, the data were fitted by pseudo-first-order (Equation (7)) and pseudo-second-order equations (Equation (8)), intraparticle diffusion (Equation (9)), and Elovich (Equation (10)).

$$\text{y} = a \times (1 - \text{e}^{(-\text{b} \times x)}) \quad (7)$$

$$\frac{t}{q_t} = \frac{1}{k_2 q_e^2} + \frac{t}{q_e} \quad (8)$$

$$q = \text{K}_\text{d} \times \text{sqrt}(t) + \text{C} \quad (9)$$

$$q_t = \ln (\text{AB})/\text{B} + (1/\text{B}) \times \ln (t) \quad (10)$$

where

A (mg/g/min) = initial rate of adsorption;
B (g/mg) = term related to the extent of surface coverage and activation energy for chemisorption;
b = rate constant;
t (min) = adsorption time;
y & q_t (mg/g) = adsorption capacity at time (t);
x = time (t);
q_e & a (mg/g) = adsorption uptake at equilibrium;
k_1 (min^{-1}) = rate constant related to pseudo first order;
k_2 (g/(mg min)) = rate constant corresponding to pseudo-second-order kinetic model;
K_d = intraparticle diffusion rate constant;
C = plot intercept implying boundary layer effect or surface adsorption.

4. Results and Discussion

4.1. Characterization

4.1.1. UV–Vis

The determination of band gap energy was performed via direct extrapolation (DE), which is normally achieved by best-fitting the straight-line curve to the linear portion of the adsorption spectrum (where $(\alpha h\nu)^2 = 0$). The determined ZnONP band gap energy was 3.172 eV (Figure 2), which is near the reported band gap energy of ~3.37 eV [85,86].

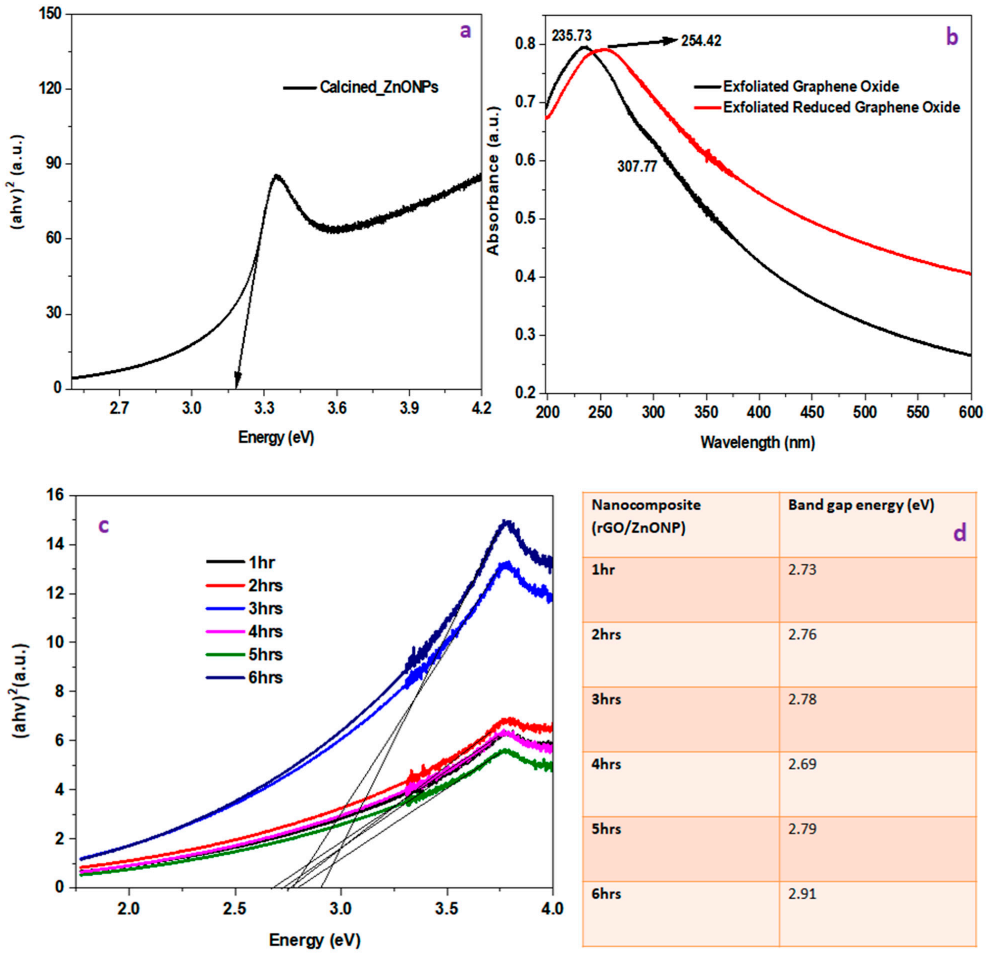

Figure 2. Tauc plot and UV–vis spectra of ZnONP, GO, rGO, and rGO/ZnONP nanocomposite. (**a**) Tauc plot of ZnONP, (**b**) UV–vis spectra of GO and rGO, (**c**) Tauc plot of rGO/ZnONP nanocomposite, (**d**) rGO/ZnONP nanocomposite and corresponding band gap energy.

Furthermore, the optical nature of rGO and GO was also monitored via UV–vis spectroscopy (Figure 2). In GO, a peak (235.73 nm) and a shoulder (307.77 nm) were observed, while only a single peak (254.42 nm) was detected in the rGO spectrum. Consequently, the adsorption peak at 235.73 nm and a shoulder at 307.77 nm constitute the aromatic C-C bonds' π-π* transition and C=O bonds' n-π* transition, implying the oxidation of the graphene sheet. In rGO, the shifting of the absorption peak is due to the aromatic C-C bonds' π-π* transition, evidence of oxygen content elimination and the disappearance of the C=O bonds' n-π* transition [87]. The optimized nanocomposite's band gap energy was the lowest when grown at 4 h (2.69 eV). This value showed that the composite may also be treated as a potential photocatalyst in addition to the adsorption behavior studied in this work.

4.1.2. FTIR

FTIR of ZnONPs, GO, rGO, and rGO/ZnONPs

Figure 3a shows the spectrum of graphene oxide with the presence of oxygen functional group stretches and vibrations at 1050, 1212, 1354, and 1710 cm^{-1} for C-O, O-H, and C=O, confirming the oxidation of graphene surfaces [88]. During the conversion to rGO, the carbon groups (C-H, C=C) were present at 1567, 2695, and 3100 cm^{-1}, revealing the restoration of sp^2-hybridized graphene structures with a noticeable elimination of oxygen functional groups (1050–1710 cm^{-1}) (as shown in Figure 2a).

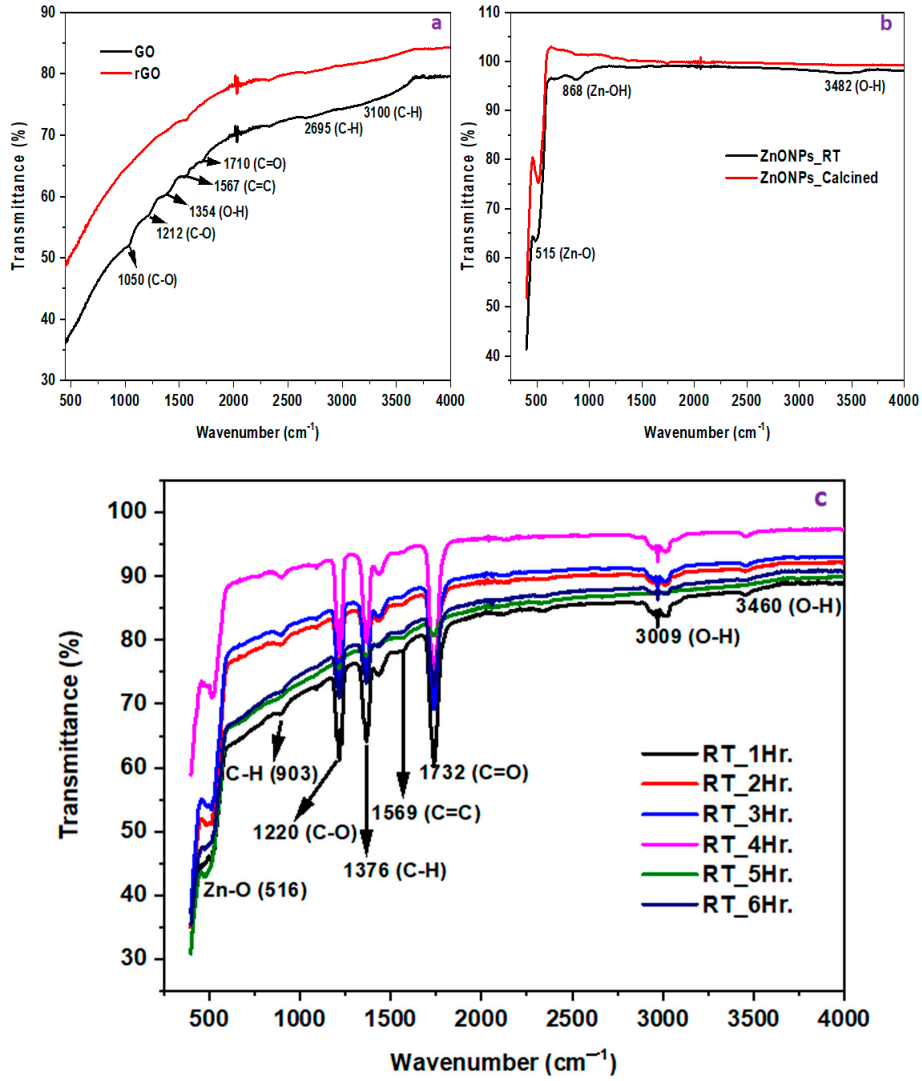

Figure 3. FTIR spectra of GO, rGO (**a**), ZnONP (**b**), and rGO/ZnONP nanocomposite (**c**).

In Figure 3b, the FT-IR spectrum of the calcined ZnONPs showed an intense and sharp peak at 515 cm^{-1}, indicating the existence of Zn-O vibrations [89]. Moreover, the hydroxyl group present in room-temperature ZnONPs at 3482 and 868 cm^{-1} was fairly eliminated, confirming the successful synthesis of ZnONPs rather than Zn-OHNPs [90].

In the case of the rGO/ZnONP nanocomposite (Figure 3c), the peak at 516 cm^{-1} indicated the stretching vibration of the ZnO [91]. The graphene sheet's structural peaks were signaled by C-H and C=C at 1376 and 1569 cm^{-1}. Furthermore, the binding of the ZnONPs onto the rGO sheets was attributed to C-O and C=O at 1220 and 1732 cm^{-1} [92]. The broad and medium stretching vibration mode at 3009 and 3460 cm^{-1} constitutes the hydroxyl group from water molecules that are absorbed on the composite surface [93]. Thus, these results have shown the formation of ZnONPs on the rGO matrix. Moreover, the optimized composite at room temperature for 4 h was selected for further characterization and subsequent metal ion removal tests. The composite showed a pronounced peak for Zn-O, signaling successful deposition as compared to other composites synthesized at room temperature (1, 2, 3, 5, and 6 h) (Figure 3c).

4.1.3. Morphology of ZnONPs and rGO/ZnONPs

TEM

Although there was a slight particle agglomeration, which could be due to the moisture exposure or incomplete solvent extraction, the ZnONPs were observed to have an almost spherical shape (Figure 4). The rGO image showed the presence of thin sheet formation and fair separation. In the composite, the surface revealed that the spherical ZnONPs were evenly distributed on the rGO surface, thus signaling a successful modification and composite output [94]. This was supported by the appearance of a new peak of a Zn–O stretch on the FTIR spectra of the synthesized rGO/ZnONP nanocomposite (Figure 3). Similar results have been documented by authors [3,95–98].

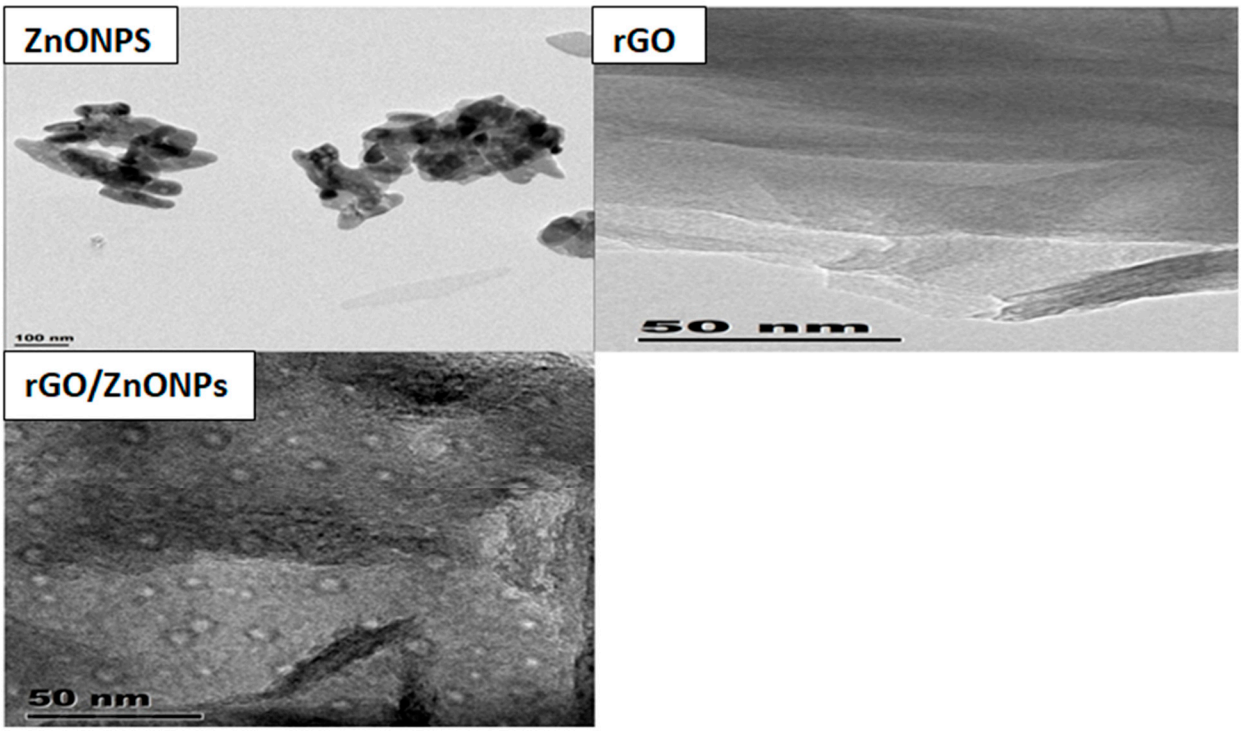

Figure 4. TEM images of rGO, ZnONPs, and rGO/ZnONPs.

4.1.4. Defect Density Study

Raman Spectra of ZnONPs and rGO/ZnONPs

The spectrum of rGO contained three prominent peaks at 1347, 1577, and 2687 cm^{-1}, which were assigned to D, G, and 2D [99]. The D and G bands were sourced from sp^2 carbon with information including the carbon pairs in a ring, the aromatic ring's breathing mode, and the defects. Amongst these bands, the G band (for sp^2 carbon structure) appeared to be sharp and with the highest intensity (~four folds of the D band). The observed D and 2D are associated with disordered crystalline carbon structural defects (oxygen and sulphur contents) and a set of the graphene sheet, respectively [100]. Five peaks were present in the ZnONPs, which are positioned at 102, 336, 440, 579, and 1151 cm^{-1}. The peak at 336 cm^{-1} was assigned to the second-order structure of ZnONPs sourced from zone boundary phonon, and 440 cm^{-1} was attributed to the E2 mode of wurtzite ZnO [101]. The weak broadband at 579 cm^{-1} was attributed to E1 (L), implying marginal defects on the ZnONP surface. The sharp peak for optical phonon E2 mode was recorded at 102 cm^{-1}, and the localized acoustic phonon mode was positioned at 50 cm^{-1} [102].

The Raman spectrum of rGO/ZnONPs is shown in Figure 5 with noticeable four bands at 10.76, 1347, 1577, and 2687 cm^{-1}. Furthermore, the reduced graphene oxide spectrum and rGO/ZnONPs showed D, G, and 2D bands at relatively the same frequency, implying that the graphene structure is fairly maintained in the composite. In the observation, the intensity of D, G, and 2D bands decreased due to the ZnONP-modified rGO surface, suggesting a successful functionalization [103]. The optical mode at 10.76 cm^{-1} is assigned to the E2 mode of the zinc and oxygen sub lattice [104].

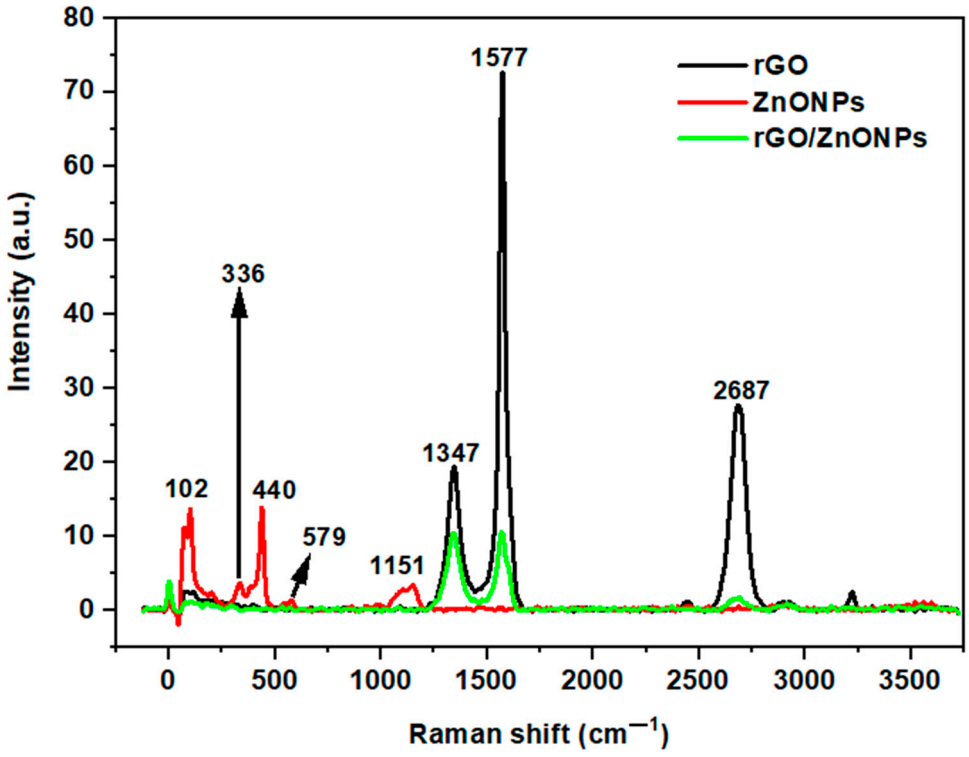

Figure 5. Raman spectra of ZnONPs, rGO, and rGO/ZnONPs.

In rGO's XRD plot (Figure 6), the sharp and strong peak at approximately 25.95° and a relatively weak intensity peak appearing at 43.59° are attributed to the reflection planes (002 and 004) of the rGO backbone [105].

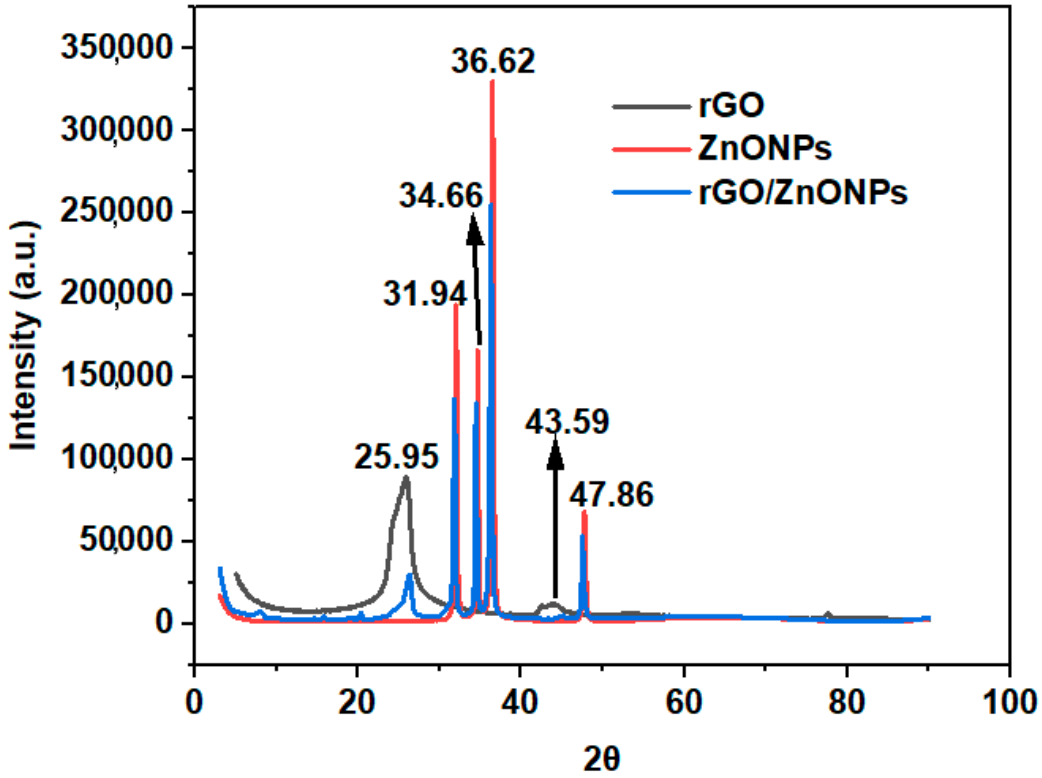

Figure 6. XRD spectra of ZnONPs, rGO, and rGO/ZnONPs.

XRD analysis was also performed to substantiate the presence of the crystalline phase identification of the standard wurtzite ZnONPs. As a result, four sharp peaks (at 31.94°, 34.66°, 36.62°, and 47.86°) were identified corresponding to 100, 002, 101, and 102 reflections [106,107]. Furthermore, the ZnONPs were observed to have fine crystalline structures due to the occurrence of stronger and sharper diffraction peaks. The average crystallite size calculated by the Debye Scherrer's equation was 22.98 nm.

There was a peak shift and appearance of low intensity of 25.95° in rGO to 26.33° in rGO/ZnONPs; this was mainly due to surface modification with the ZnONPs. The crystallinity of the rGO/ZnONPs was also observed due to prominent and sharp peak presence; this was mainly sourced from the ZnONP crystallinity [108].

4.2. Removal Study

4.2.1. Adsorption Performance

For the determination of adsorption efficiency, the initial pH is an essential aspect because it includes the principal interaction between the adsorbent and adsorbate species. At various pH numbers, the activity and concentration of the hydronium (H^+) and hydroxyl group (OH^-) tend to be different, and this may have an impact on electrostatic interaction between the adsorbent surface and adsorbates, being one of the adsorption mechanisms. Consequently, the effect of pH on the adsorption capacity of Pb (II) and Cd (II) using rGO/ZnONPs was investigated from pH 3 to 9 (Figure 7). For the Pb adsorption at pH 3 (19.75 mg/g) and 4 (19.91 mg/g), the adsorption capacities were lower than at pH 5 (20.00 mg/g); this could be due to the enhanced adsorbent surface protonation (more acidic), which possibly led to the hindrance of oxygenated functional group protonation and less Pb^{2+} adsorption sites, thus leading to repulsive interaction between the H^+ and Pb^{2+} at pH 3 and 4. Moreover, at pH 6 and 7, the adsorption performance decreased drastically due to the gradual insolubility of Pb, resulting in possible hydroxide precipitation, which may be $Pb(OH)_2$(s), $Pb_4(OH_4)^{2+}$(s), $Pb_4(OH_4)^{4+}$(s), and $Pb_6(OH_8)^{4+}$(s) [109].

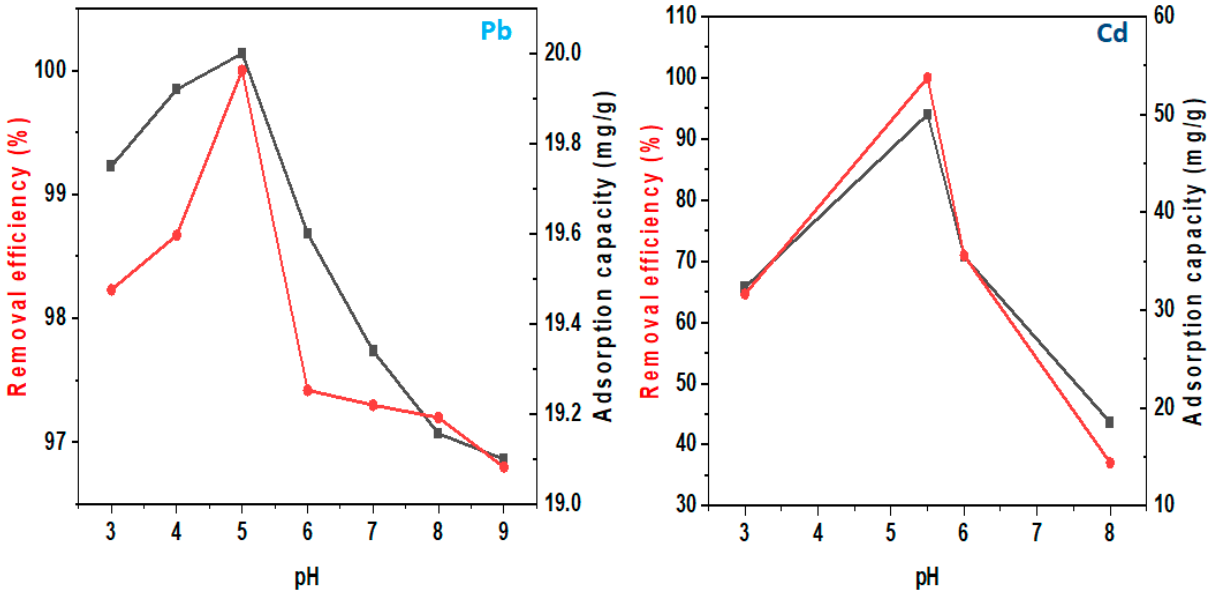

Figure 7. pH study for the adsorption of Pb and Cd by rGO/ZnONPs.

Cd adsorption was favored by pH 5.5, implying that the adsorbates' transport within the adsorbent surface outperformed the presence of hydronium (H^+) ion in the acidic phase and hydroxyl group (OH^-) in the alkaline level. This resulted in the maximum removal capacity and efficiency of 49.99 mg/g and 99.99%. The implication was that the alkaline pH may be avoided because of the inactivity of adsorption and enhanced precipitation, which may result in secondary pollution (sludge formation). Thus, the removal of Pb^{2+} and Cd^{2+} is the least efficient at a more basic pH = 9 (19.09 mg/g) and 8 (18.51 mg/g). Conclusively, the optimum adsorption pH was found to be 5 and 5.5 for Pb^{2+} and Cd^{2+}.

Furthermore, Figure 8 illustrates Pb^{2+} and Cd^{2+} metal uptake using various adsorbent dosages (5–50 mg). During the Pb^{2+} adsorption, it can be seen that rapid adsorption took place from 5 to 15 mg due to the occupation of available surface sites. When 15 mg of rGO/ZnONPs was utilized for sorption, the Pb^{2+} removal capacity reached a maximum of 19.98 mg/g. From 15 to 25 mg dosage, the process had equilibrium characteristics, thus indicating the excessive site state for the studied 3 ppm. Hence, the 15 mg seemed to be the optimum rGO/ZnONP dosage for Pb (II) adsorption. However, at 25 to 50 mg, there was a depreciation of removal efficiency on the adsorbent surface, and this may be sourced from the slight desorption (physisorption characteristic), stirring effect, and competition of sites amongst the H^+ and Pb^{2+}.

From 5 to 15 mg, there was a decrease in removal efficiency from 59.37 to 53.55 mg/g. This could be sourced from the unavailability of uptake sites related to H^+ and Cd^{2+} ion concentration. However, the efficiency increased from 15 mg with the maximum removal efficiency related to Cd^{2+}, recorded as 73.13%, using 50 mg. Afterwards, there was a slight decrease in efficiency from 50 to 85 mg, and the source may be the excess site preoccupied by H^+ ion and Cd^{2+} site competition.

An increase in adsorbent dosage resulted in a decrease in adsorption capacity; this could be due to net active sites being available at lower doses, whereas only active sites were exposed at larger doses. Therefore, high adsorbent dose usage could result in sudden material aggregation and, thus, decrease the material's net surface area, pore volumes, and sizes, which would result in a decrease in adsorption performance [110].

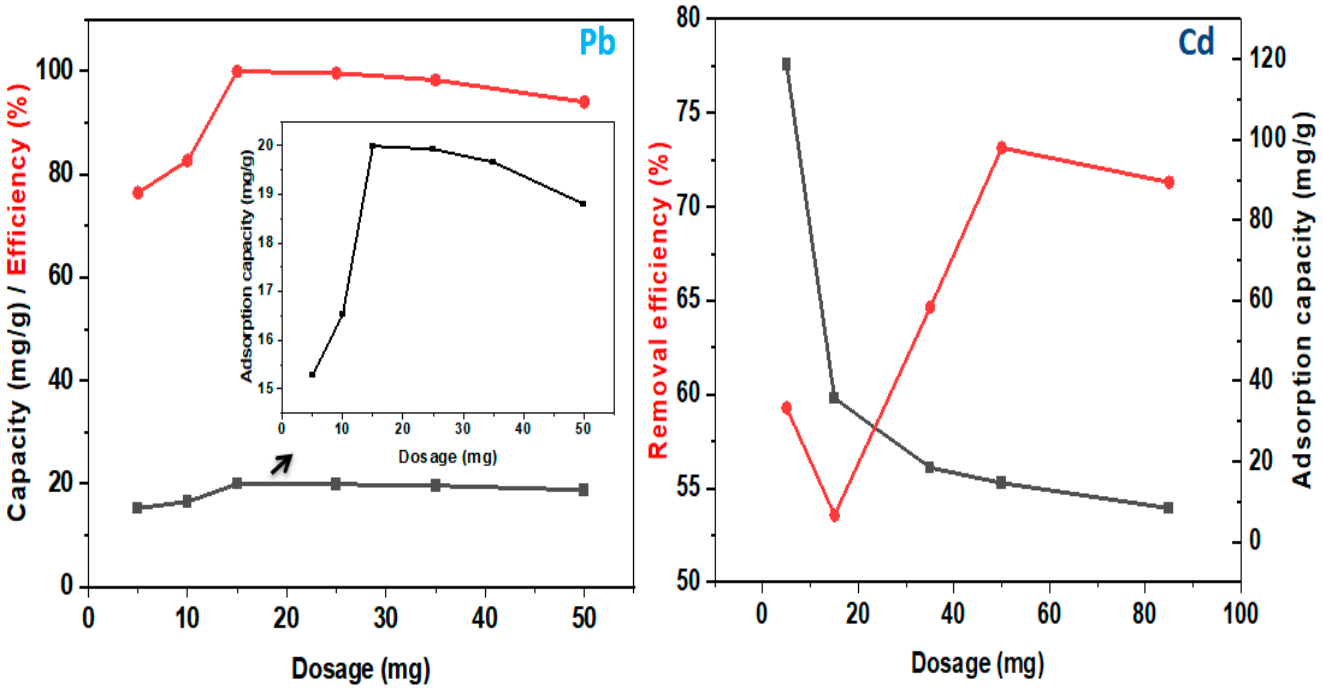

Figure 8. Dosage study for the adsorption of Pb and Cd by rGO/ZnONPs.

The adsorbent's available site to adsorbate concentration ratio is key for adsorption, especially in signaling the saturation/unsaturated site relations and equilibrium state. Consequently, Figure 9 shows the study of the concentration of Pb^{2+} and Cd^{2+} (3–60 ppm). For Pb^{2+} removal, the trend implied a proportional increment of both the initial concentration and corresponding removal capacity even at a maximum of 50 ppm with 242.013 mg/g. However, the removal efficiency moderately decreased with increased concentrations since the surface occupation was gradually reaching the maximum uptake level with the order: 50 < 40 < 30 < 25 < 10 < 3 ppm = 72.60 < 81.080 < 88.87 < 91.92 < 89.85 < 99.99%.

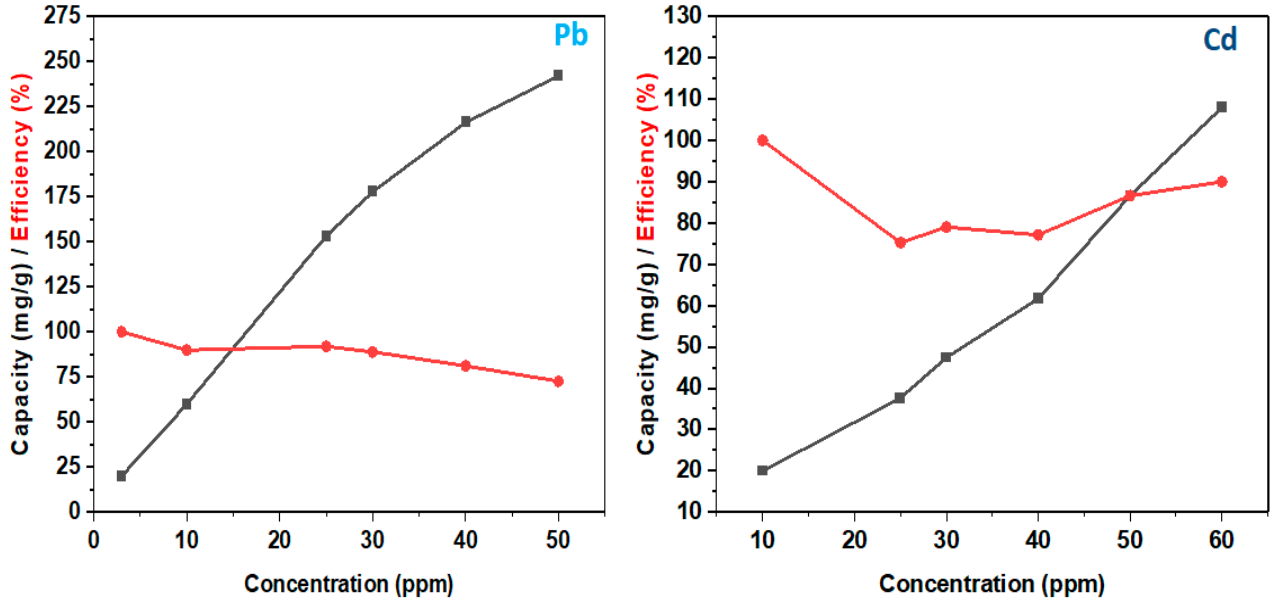

Figure 9. Concentration study for the adsorption of Pb and Cd by rGO/ZnONPs.

During the Cd^{2+} removal, the adsorption capacity increased with an increase in concentration, implying that the adsorbent had active binding sites for Cd^{2+}. However, the

removal efficiency decreased from 99.79 to 89.84%, possibly because of the desorption and the unavailability of sufficient adsorption sites [111].

Various treatment environments deal with different pollutants with specific temperatures. Therefore, the temperature effect on adsorption performance towards incoming adsorbate species was investigated. Figure 10 shows the temperature study on the adsorption of Pb^{2+} and Cd^{2+}. An inverse proportional relationship between the temperature (25–100 °C) and adsorption performance was observed. Evidently, there were maximum capacity (19.82 and 49.93 mg/g) and efficiency (99.073 and 99.86%) at 25 °C as compared to the lower levels of the minimum capacity (9.66 and 35.60 mg/g) and efficiency (48.28 and 55.79%) at 100 °C for Pb^{2+} and Cd^{2+}. This observation could be due to an increased temperature (heat deposition) disturbing the surface adsorption mechanism between the adsorbent and adsorbate ions. Therefore, the optimum temperature was found to be 25 °C.

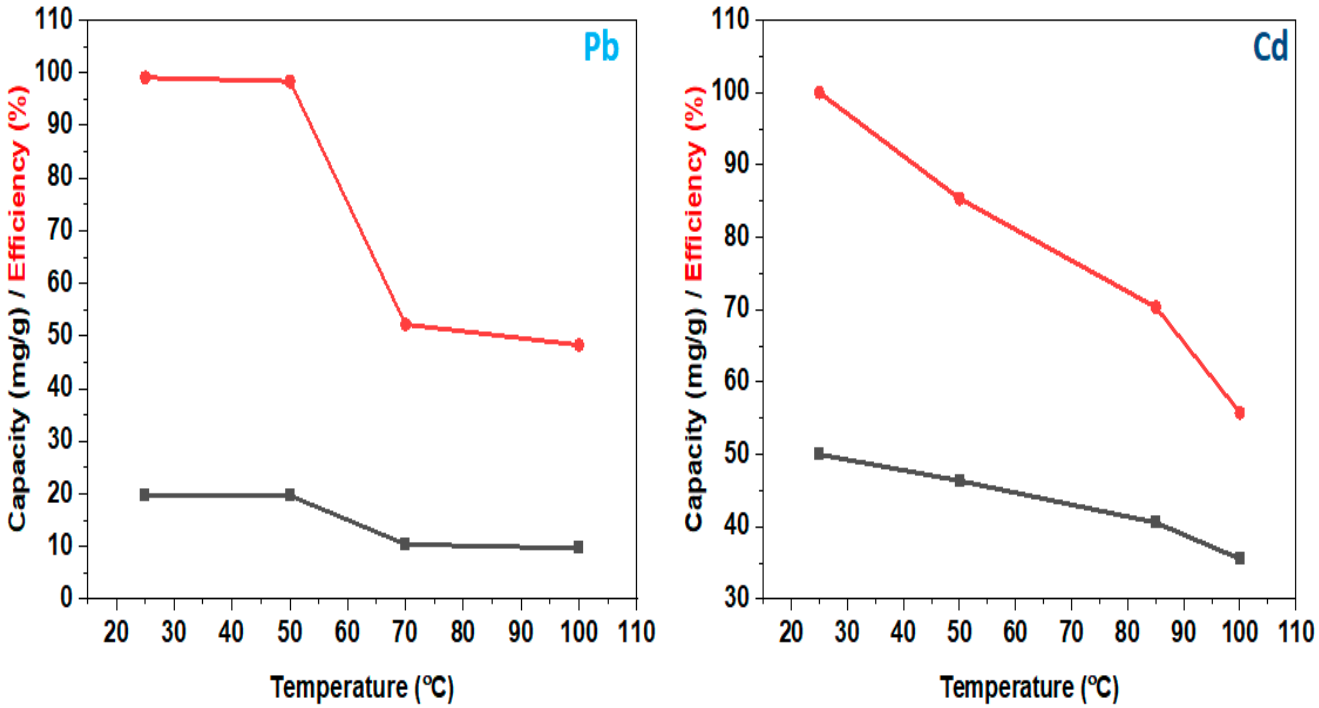

Figure 10. Temperature study for the adsorption of Pb and Cd by rGO/ZnONPs.

Additionally, since the adsorption is partitioned into two phases (rapid and equilibrium), the contact-time study was conducted to determine the generation of each phase. As a result, Figure 11 shows the investigated Pb^{2+} and Cd^{2+} removal from 0–240 min. Rapid adsorption was seen from 0–90 min (due to active site abundance), and the equilibrium plateau clocked at 90–240 min, showing the maximum adsorption (19.99 mg/g; 99.96%) for Pb^{2+} uptake. On the other hand, there was a rapid Cd^{2+} removal in a short period of 10 min, and equilibrium was quickly reached too, thus making fast kinetic rates characteristic.

The life cycle assessment of adsorbents is dependent on adsorbent synthesis, method costs, and secondary waste management to meet consistent desorption–adsorption trials [112].

As a result, Figure 12 shows the uptake efficiency of Pb^{2+} and Cd^{2+} in multiple cycles using rGO/ZnONPs. The use of H_2SO_4 solution allowed for successful desorption and recovery and reuse of rGO/ZnONPs. The material may reach half of its removal efficiency after seven desorption cycles. The maximum efficiency achieved at cycle 1 was 99.96%, and the lowered efficiency was 52.21%, for Pb^{2+}.

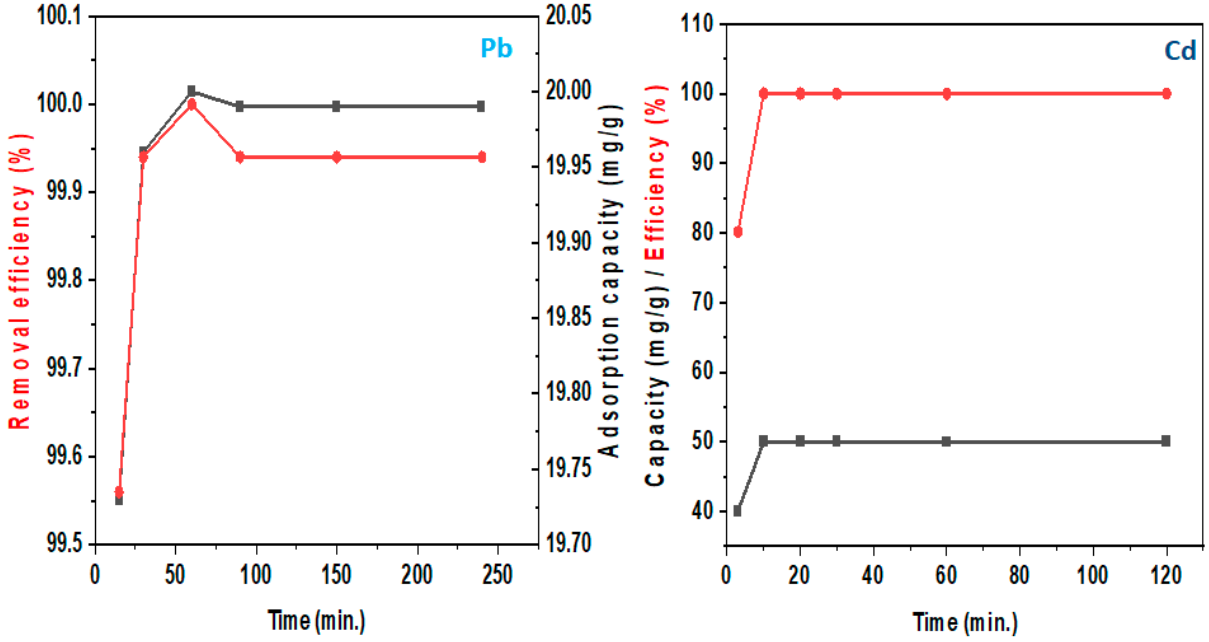

Figure 11. Contact-time study for the adsorption of Pb and Cd by rGO/ZnONPs.

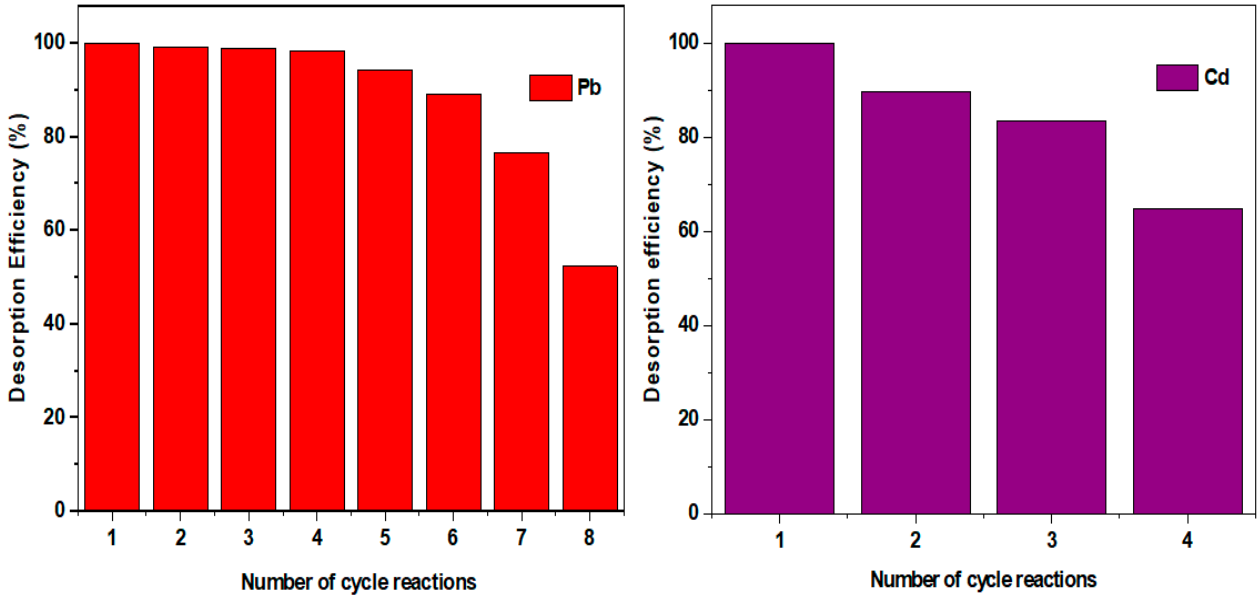

Figure 12. Number of succeeding cycles for adsorption of Pb and Cd by rgo/ZnONPs.

In the case of Cd^{2+} removal, the material supported three successive desorption efficiencies for almost half of the performance of the uptake. This could be attributed to the unavailability of sites, enhanced population of Cd^{2+}, lack of magnetism, low acid strength for desorption, and loss of structural material formation (surface area and porosity) [113,114].

The observed removal efficiency trend was Cu > Cr > Fe > Pb > Cd > Zn (Figure 13). The rgo/ZnONP nanocomposite showed an affinity towards Cu, Fe, Cr, Cd, and Pb, unlike the Zn removal efficiency. This constitutes selectivity and specificity towards the five metal ions [115]. The rgo/ZnONP nanocomposite's lowest adsorption performance for Zn metal adsorption may be attributed to the undesirable used contact time, concentration, temperature, agitation speed, and pH, thus leading to poor transport to and within the adsorbent active surface sites or quick and spontaneous desorption after a possible physisorption phase [116,117].

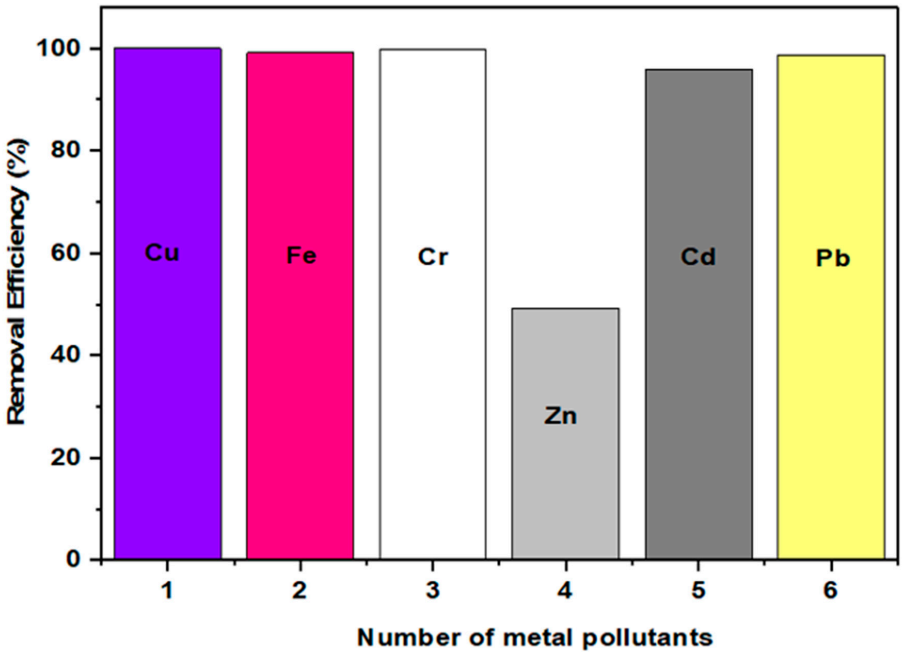

Figure 13. Simultaneous removal for adsorption of toxic metals in wastewater by rgo/ZnONPs.

4.2.2. Adsorption Mechanism

The adsorption experimental data were fitted using the Langmuir, Freundlich, Temkin, and Sips isotherm models, and the corresponding parameters are summarized in Table 2. After an investigation of the adsorption factors, the results showed a best fit by using the Freundlich model (R^2~1) with an unfavorable fit related to the Sips, Langmuir, and Temkin isotherm models for Pb (II) adsorption (Figure 14). The Freundlich model assumes multilayer adsorption, that is, the adsorbed layer is only multiple molecules in thickness, so adsorption can only occur at an infinite number of sites and at the heterogeneous adsorbent surface (physisorption characteristic). Multiple studies have been conducted with the use of graphene–zinc oxide composites for Pb (II) uptake, where Freundlich was dominant over the other isotherm models.

Table 2. Parameters of the Freundlich, Sips, Temkin, and Langmuir isotherms for Pb (II) and Cd (II) adsorption.

Pollutant	Isotherm Model	Parameter	
Pb (II)	Langmuir	q_{max}	242.0133
		K_L	−4424.779
		R^2	−1.319
	Freundlich	n	0.345
		K_f	0.479
		R^2	0.915
	Temkin	B	18.00530
		A_t	427.121
		R^2	0.698
	Sips	q_m	19.552
		K	1.368
		n	0.687
		R^2	−2.447

Table 2. *Cont.*

Pollutant	Isotherm Model	Parameter	
Cd (II)	Langmuir	q_{max}	50.003
		K_L	−2.510
		R^2	0.350
	Freundlich	n	0.143
		K_f	39.0222
		R^2	0.838
	Temkin	B	4.255
		A_t	20.357
		R^2	0.952
	Sips	q_m	49.999
		K	0.7
		n	50.734
		R^2	0.999

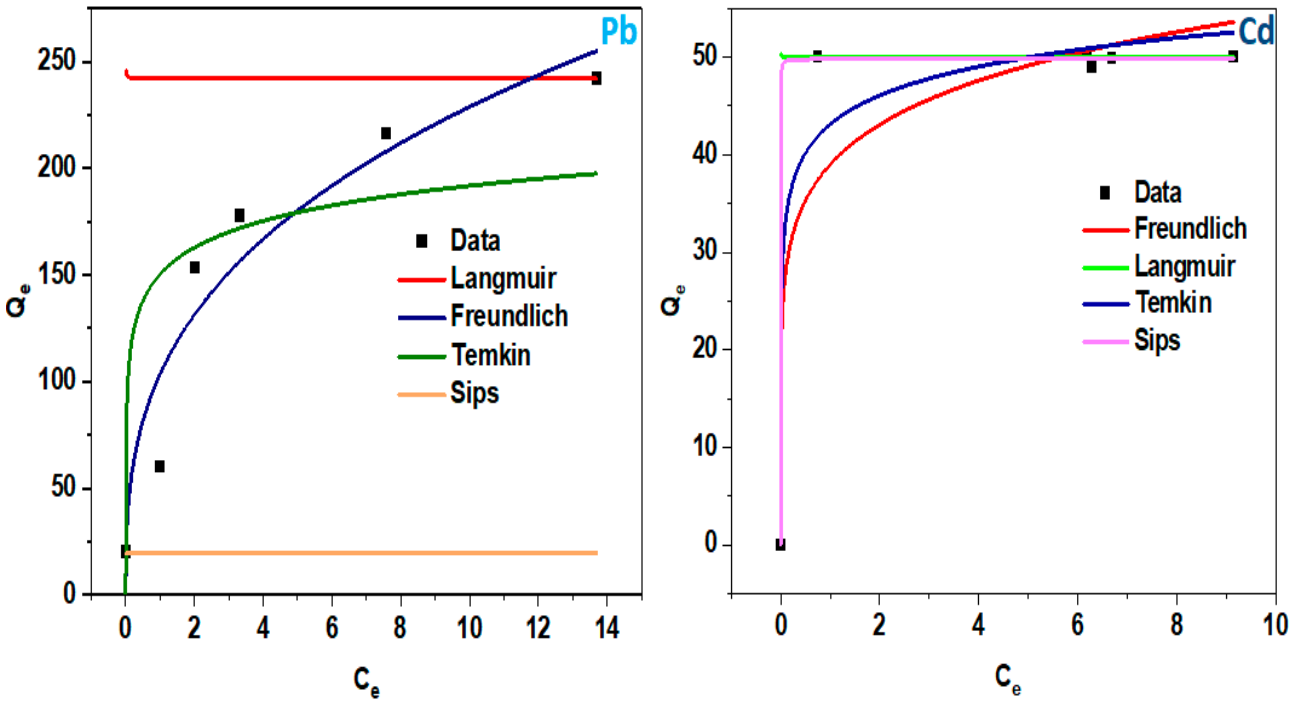

Figure 14. Isotherm plot of Langmuir, Freundlich, Temkin, and Sips for Pb (II) and Cd (II) adsorption.

During the Cd (II) adsorption, it can be observed that the isotherm data were well fitted by the Sips adsorption model (R^2 = 0.999) as compared to others. Since the model is a hybrid of Langmuir and Freundlich, this implies that the adsorption can fairly be described by Freundlich behavior (multilayer adsorption with physical interaction) at low concentrations and be favorable to the Langmuir (monolayer adsorption with chemical interaction) model at adsorbate high concentration.

4.2.3. Kinetic Models

Figure 15 showed the best fit with the correlation coefficient of pseudo first order being favored (R^2 = 0.99) and followed by descending order of Elovich < intraparticle diffusion <

pseudo second order. From the models, the adsorbate's constant uptake rate and interaction with the contact time at the interface of solid and solution could be quantified [118]. In terms of the pseudo-first-order model, the assumption is that the adsorption site occupying rate is correlated to the number of unoccupied sites [119]. The (R^2) of this model is ~1. It depicted that the adsorption had occurred through physisorption, which is in correlation with the Freundlich isotherm of Pb (II) adsorption [118]. In the case of the Cd (II) adsorption, the kinetic data were favored by pseudo first order with R^2 = 0.999 and b = 0.538 as compared to pseudo second order (R^2 = 0.905), Elovich (R^2 = 0.322), and intraparticle diffusion (R^2 = 0.323). The alignment with pseudo first order constitutes a fast kinetic rate and affinitive surface for Cd (II). The lowest correlation coefficient related to Elovich also constitutes that chemisorption (a partial characteristic of the Sips model) was involved in the metal uptake [120].

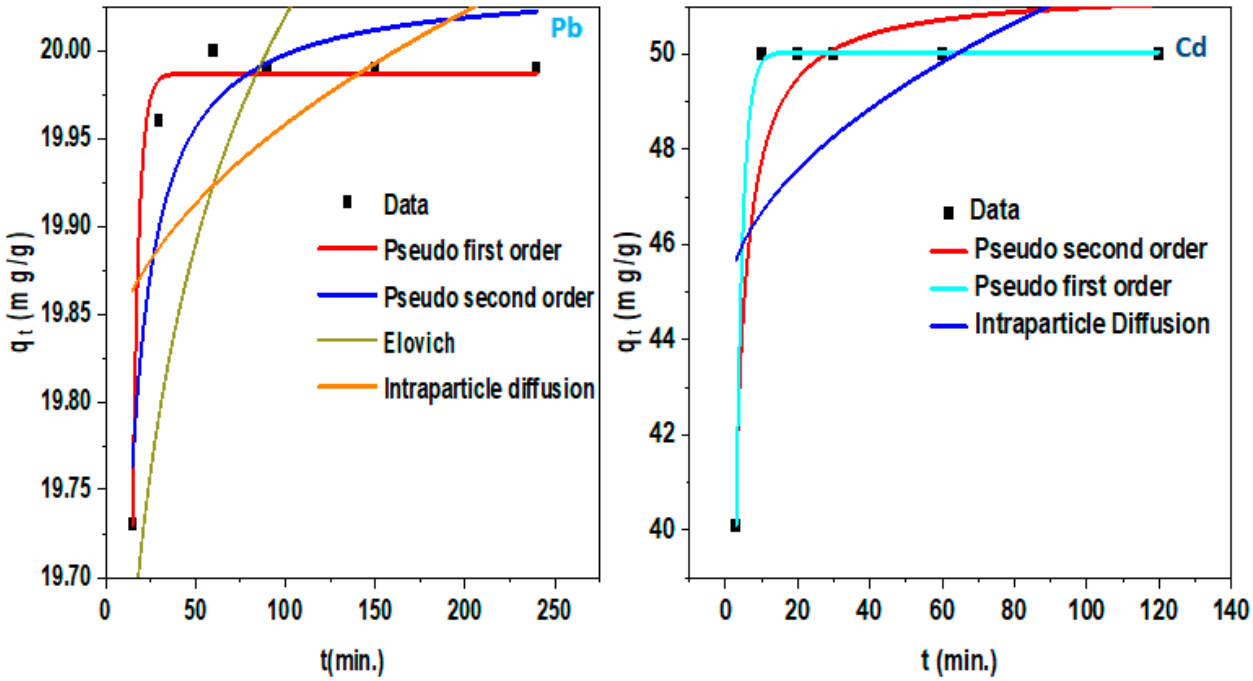

Figure 15. Kinetic study by pseudo first, pseudo second, Elovich, and intraparticle diffusion for Pb(II) adsorption.

5. Conclusions

The current investigation has shown the possibility of applying a simple and straightforward method in the development of rGO/ZnONP nanocomposite. The synthesis was carried out for 4 h at room temperature and in an inert environment. It was observed that the synthesized nanocomposite has the potential as a multifunctional material (photoactive and adsorptive capability). Furthermore, pronounced peaks in FTIR and Raman spectra have shown the successful functionalization of reduced graphene oxide surface with minimal defects while fairly retaining the sp^2 carbon of the support material. Afterward, the crystalline nanocomposite was tested for adsorption of Pb (II) and Cd (II) in wastewater. The observation showed that the optimized equilibrium contact times (10; 90 min), pH (5; 5.5), temperature (25 °C), adsorbent dose (15; 50 mg), and initial concentrations (3; 10 mg/L) were achieved for Pb (II) and Cd (II) uptake with corresponding adsorption capacity (19.99; 49.99 mg/g) and removal efficiency (~100%) for Pb (II) and Cd (II) removal.

Furthermore, the adsorption behavior was monitored by isotherm and kinetic study. Both studies revealed favoritism of pseudo first order with Pb and Cd isotherm related to the Freundlich and Sips adsorption models, respectively. As a result, the possible adsorption mechanisms are due to the presence of strong ionic bonding and electrostatic interactions involving the dipole–dipole moment between the oxygen group of the supported

ZnO nanoparticle and the adsorbate (Cd (II) and Pb (II)). Furthermore, the electronegativity of the nanocomposites proved to be accommodating to co-existing metals (with efficiency > 90%); thus, this can potentially act as a multifunctional cation adsorbate remover. The rGO/ZnONP nanocomposite also proved to support the desorption and reuse mode with considerable removal efficiencies, especially during Pb (II) adsorption (seven successive cycles towards half material efficiency) as compared to Cd (II) adsorption (three successive cycles towards half material efficiency), and this could be improved by combatting the leaching of the material by further functionalization with a capping agent. Conclusively, the functionalized rGO/ZnONP nanocomposite could act as a potential material for contaminant (not necessarily toxic metals) removal in wastewater. Therefore, this nanocomposite presents the simple route of surface tuning and is efficient, reusable, and less energy consuming. It also possesses technical feasibility in affinitive adsorbent production for wastewater treatment.

6. Recommendations/Future Perspectives

Although there are multiple prospects for nanocomposites and nanomaterials, such as high adsorption capacity and efficiency, tunable surface for various functionalities, and porosity, challenges like durability, harsh chemical use for pH adjustment, specificity, selectivity, real-world practical application, scaling up, long-term stability, regeneration, and reusability are still yet to be deeply researched. Additionally, thorough concentration should be channeled into understanding the effect of shape, particle size, surface pore diameter and volume, surface area, adsorbent type, and material's stability on the adsorption thermodynamics and kinetics models, engineering efficient and sustainable adsorbents and various adsorption phases for the removal of toxic metal ion in wastewater. Although the treatment of real wastewater from industries may require large amounts of adsorbing material, the focus should be on the up-scaled production of adsorbents while maintaining low cost, low energy consumption, reproducibility, and stable compatibility in wastewater treatment plants.

Author Contributions: Conceptualization, K.O.B.; methodology, M.G.M.; validation, L.K.; writing-original Draft, M.G.M.; writing—review and editing: K.O.B.; supervision: L.K. All authors have read and agreed to the published version of the manuscript.

Funding: The National Research Foundation (NRF), grant number (138079) and Eskom, grant number (2002/015527/0), South Africa.

Data Availability Statement: The original data presented in the study are openly available in the University of the Western Cape repository at https://repository.uwc.ac.za/ (accessed on 18 June 2024).

Conflicts of Interest: The authors declare no conflicts of interest.

References

1. Kumar, S.; Prasad, S.; Yadav, K.K.; Shrivastava, M.; Gupta, N.; Nagar, S.; Bach, Q.V.; Kamyab, H.; Khan, S.A.; Yadav, S.; et al. Hazardous heavy metals contamination of vegetables and food chain: Role of sustainable remediation approaches—A review. *Environ. Res.* **2019**, *179*, 108792. [CrossRef] [PubMed]
2. Khalid, S.; Shahid, M.; Natasha; Shah, A.H.; Saeed, F.; Ali, M.; Qaisrani, S.A.; Dumat, C. Heavy metal contamination and exposure risk assessment via drinking groundwater in Vehari, Pakistan. *Environ. Sci. Pollut. Res.* **2020**, *10*, 39852–39864. [CrossRef]
3. Gulati, A.; Mandeep; Malik, J.; Kakkar, R. Mesoporous rGO@ZnO composite: Facile synthesis and excellent water treatment performance by pesticide adsorption and catalytic oxidative dye degradation. *Chem. Eng. Res. Des.* **2020**, *160*, 254–263. [CrossRef]
4. Lee, X.J.; Hiew, B.Y.Z.; Lai, K.C.; Lee, L.Y.; Gan, S.; Thangalazhy-Gopakumar, S.; Rigby, S. Review on graphene and its derivatives: Synthesis methods and potential industrial implementation. *J. Taiwan Inst. Chem. Eng.* **2019**, *98*, 163–180. [CrossRef]
5. Ahmad, S.Z.N.; Wan Salleh, W.N.; Ismail, A.F.; Yusof, N.; Mohd Yusop, M.Z.; Aziz, F. Adsorptive removal of heavy metal ions using graphene-based nanomaterials: Toxicity, roles of functional groups and mechanisms. *Chemosphere* **2020**, *248*, 126008. [CrossRef]
6. Tchounwou, P.B.; Yedjou, C.G.; Patlolla, A.K.; Sutton, D.J. Heavy Metal Toxicity and the Environment. In *Molecular, Clinical and Environmental Toxicology*; Luch, A., Ed.; Springer: Basel, Switzerland, 2012; Volume 101, pp. 133–164. [CrossRef]

7. Türkmen, D.; Bakhshpour, M.; Akgönüllü, S.; Aşır, S.; Denizli, A. Heavy Metal Ions Removal From Wastewater Using Cryogels: A Review. *Front. Sustain.* **2022**, *3*, 765592. [CrossRef]
8. Assi, M.A.; Hezmee, M.N.M.; Haron, A.W.; Sabri, M.Y.M.; Rajion, M.A. The detrimental effects of lead on human and animal health. *Vet. World* **2016**, *9*, 660–671. [CrossRef] [PubMed]
9. Collin, S.; Baskar, A.; Geevarghese, D.M.; Ali, M.N.V.S.; Bahubali, P.; Choudhary, R.; Lvov, V.; Tovar, G.I.; Senatov, F.; Koppala, S.; et al. Bioaccumulation of lead (Pb) and its effects in plants: A review. *J. Hazard. Mater. Lett.* **2022**, *3*, 100064. [CrossRef]
10. Ahmed, S.; Uddin, M.F.; Hossain, M.S.; Jubair, A.; Islam, M.N.; Rahman, M. Heavy metals contamination in shrimp and crab from southwest regions in Bangladesh: Possible health risk assessment. *Toxicol. Rep.* **2023**, *10*, 580. [CrossRef]
11. Huff, J.; Lunn, R.M.; Waalkes, M.P.; Tomatis, L.; Infante, P.F. Cadmium-induced cancers in animals and in humans. *Int. J. Occup. Environ. Health* **2007**, *13*, 202–212. [CrossRef]
12. Haider, F.U.; Liqun, C.; Coulter, J.A.; Cheema, S.A.; Wu, J.; Zhang, R.; Wenjun, M.; Farooq, M. Cadmium toxicity in plants: Impacts and remediation strategies. *Ecotoxicol. Environ. Saf.* **2021**, *211*, 111887. [CrossRef] [PubMed]
13. Burakov, A.E.; Galunin, E.V.; Burakova, I.V.; Kucherova, A.E.; Agarwal, S.; Tkachev, A.G.; Gupta, V.K. Adsorption of heavy metals on conventional and nanostructured materials for wastewater treatment purposes: A review. *Ecotoxicol. Environ. Saf.* **2018**, *148*, 702–712. [CrossRef] [PubMed]
14. Bankole, M.T.; Abdulkareem, A.S.; Mohammed, I.A.; Ochigbo, S.S.; Tijani, J.O.; Abubakre, O.K.; Roos, W.D. Selected Heavy Metals Removal from Electroplating Wastewater by Purified and Polyhydroxylbutyrate Functionalized Carbon Nanotubes Adsorbents. *Sci. Rep.* **2019**, *9*, 4475. [CrossRef]
15. Topare, N.S.; Wadgaonkar, V.S. A review on application of low-cost adsorbents for heavy metals removal from wastewater. *Mater. Today Proc.* **2023**, *77*, 8–18. [CrossRef]
16. Heidari, A.; Younesi, H.; Mehraban, Z.; Heikkinen, H. Selective adsorption of Pb(II), Cd(II), and Ni(II) ions from aqueous solution using chitosan-MAA nanoparticles. *Int. J. Biol. Macromol.* **2013**, *61*, 251–263. [CrossRef] [PubMed]
17. Alalwan, H.A.; Kadhom, M.A.; Alminshid, A.H. Removal of heavy metals from wastewater using agricultural byproducts. *J. Water Supply Res. Technol.—AQUA* **2020**, *69*, 99–112. [CrossRef]
18. Zhang, H.; Zhang, Y.; Pan, Y.; Wang, F.; Sun, Y.; Wang, S.; Wang, Z.; Wu, A.; Zhang, Y. Efficient removal of heavy metal ions from wastewater and fixation of heavy metals in soil by manganese dioxide nanosorbents with tailored hollow mesoporous structure. *Chem. Eng. J.* **2023**, *459*, 141583. [CrossRef]
19. Albqmi, M.; Frontistis, Z.; Raji, Z.; Karim, A.; Karam, A.; Khalloufi, S. Adsorption of Heavy Metals: Mechanisms, Kinetics, and Applications of Various Adsorbents in Wastewater Remediation—A Review. *Waste* **2023**, *1*, 775–805. [CrossRef]
20. Kreyling, W.G.; Semmler-Behnke, M.; Chaudhry, Q. A complementary definition of nanomaterial. *Nano Today* **2010**, *5*, 165–168. [CrossRef]
21. Khan, I.; Saeed, K.; Khan, I. Nanoparticles: Properties, applications and toxicities. *Arab. J. Chem.* **2019**, *12*, 908–931. [CrossRef]
22. Subramaniam, M.N.; Goh, P.S.; Lau, W.J.; Ismail, A.F. The roles of nanomaterials in conventional and emerging technologies for heavy metal removal: A state-of-the-art review. *Nanomaterials* **2019**, *9*, 625. [CrossRef] [PubMed]
23. Babel, S.; Kurniawan, T.A. Low-cost adsorbents for heavy metals uptake from contaminated water: A review. *J. Hazard. Mater.* **2003**, *97*, 219–243. [CrossRef] [PubMed]
24. Pehlivan, E.; Cetin, S.; Yanik, B.H. Equilibrium studies for the sorption of zinc and copper from aqueous solutions using sugar beet pulp and fly ash. *J. Hazard. Mater.* **2006**, *135*, 193–199. [CrossRef] [PubMed]
25. Guerra, D.L.; Airoldi, C.; de Sousa, K.S. Adsorption and thermodynamic studies of Cu(II) and Zn(II) on organofunctionalized-kaolinite. *Appl. Surf. Sci.* **2008**, *254*, 5157–5163. [CrossRef]
26. Irannajad, M.; Kamran Haghighi, H. Removal of Heavy Metals from Polluted Solutions by Zeolitic Adsorbents: A Review. *Environ. Process.* **2021**, *8*, 7–35. [CrossRef]
27. Fouda-Mbanga, B.G.; Prabakaran, E.; Pillay, K. Carbohydrate biopolymers, lignin based adsorbents for removal of heavy metals (Cd^{2+}, Pb^{2+}, Zn^{2+}) from wastewater, regeneration and reuse for spent adsorbents including latent fingerprint detection: A review. *Biotechnol. Rep.* **2021**, *30*, e00609. [CrossRef]
28. Smith, A.T.; LaChance, A.M.; Zeng, S.; Liu, B.; Sun, L. Synthesis, properties, and applications of graphene oxide/reduced graphene oxide and their nanocomposites. *Nano Mater. Sci.* **2019**, *1*, 31–47. [CrossRef]
29. Khoso, W.A.; Haleem, N.; Baig, M.A.; Jamal, Y. Synthesis, characterization and heavy metal removal efficiency of nickel ferrite nanoparticles (NFN's). *Sci. Rep.* **2021**, *11*, 3790. [CrossRef]
30. Zaidi, R.; Khan, S.U.; Azam, A.; Farooqi, I.H. A study on effective adsorption of lead from an aqueous solution using Copper Oxide nanoparticles. *IOP Conf. Ser. Mater. Sci. Eng.* **2021**, *1058*, 012074. [CrossRef]
31. Del Prado-Audelo, M.L.; García Kerdan, I.; Escutia-Guadarrama, L.; Reyna-González, J.M.; Magaña, J.J.; Leyva-Gómez, G. Nanoremediation: Nanomaterials and Nanotechnologies for Environmental Cleanup. *Front. Environ. Sci.* **2021**, *9*, 793765. [CrossRef]
32. Bian, S.W.; Mudunkotuwa, I.A.; Rupasinghe, T.; Grassian, V.H. Aggregation and dissolution of 4 nm ZnO nanoparticles in aqueous environments: Influence of pH, ionic strength, size, and adsorption of humic acid. *Langmuir* **2011**, *27*, 6059–6068. [CrossRef]
33. Phan, H.T.; Haes, A.J. What Does Nanoparticle Stability Mean? *J. Phys. Chem. C* **2019**, *123*, 16495–16507. [CrossRef] [PubMed]

34. Velempini, T.; Ahamed, M.E.H.; Pillay, K. Heavy-metal spent adsorbents reuse in catalytic, energy and forensic applications- a new approach in reducing secondary pollution associated with adsorption. *Results Chem.* **2023**, *5*, 100901. [CrossRef]
35. Kim, J.; Lee, K.; Seo, B.K.; Hyun, J.H. Effective removal of radioactive cesium from contaminated water by synthesized composite adsorbent and its thermal treatment for enhanced storage stability. *Environ. Res.* **2020**, *191*, 110099. [CrossRef] [PubMed]
36. Contreras, A.R.; Casals, E.; Puntes, V.; Komilis, D.; Sánchez, A.; Font, X. Use of cerium oxide (CeO_2) nanoparticles for the adsorption of dissolved cadmium (II), lead (II) and chromium (VI) at two different pHs in single and multi-component systems. *Glob. Nest J.* **2015**, *17*, 536–543.
37. Dave, P.N.; Chopda, L.V. Application of iron oxide nanomaterials for the removal of heavy metals. *J. Nanotechnol.* **2014**, *2014*, 1–14. [CrossRef]
38. Dhiman, V.; Kondal, N. ZnO Nanoadsorbents: A potent material for removal of heavy metal ions from wastewater. *Colloids Interface Sci. Commun.* **2021**, *41*, 100380. [CrossRef]
39. Sosun; Ali, A.; Mannan, A.; Ali Shah, U.; Zia, M. Removal of of toxic metal ions (Ni^{2+} and Cd^{2+}) from wastewater by using TOPO decorated iron oxide nanoparticles. *Appl. Water Sci.* **2022**, *12*, 86. [CrossRef]
40. Al-Mur, B.A. Green Zinc Oxide (ZnO) Nanoparticle Synthesis Using Mangrove Leaf Extract from Avicenna marina: Properties and Application for the Removal of Toxic Metal Ions (Cd^{2+} and Pb^{2+}). *Water* **2023**, *15*, 455. [CrossRef]
41. Shaba, E.Y.; Jacob, J.O.; Tijani, J.O.; Suleiman, M.A.T. A critical review of synthesis parameters affecting the properties of zinc oxide nanoparticle and its application in wastewater treatment. *Appl. Water Sci.* **2021**, *11*, 48. [CrossRef]
42. Thi Le, A.; Pung, S.-Y.; Sreekantan, S.; Matsuda, A.; Phu Huynh, D.; Phu Huynh Mechanisms, D. Mechanisms of removal of heavy metal ions by ZnO particles. *Heliyon* **2019**, *5*, 1440. [CrossRef]
43. Naseem, T.; Durrani, T. The role of some important metal oxide nanoparticles for wastewater and antibacterial applications: A review. *Environ. Chem. Ecotoxicol.* **2021**, *3*, 59–75. [CrossRef]
44. Chaüque, E.F.C.; Zvimba, J.N.; Ngila, J.C.; Musee, N. Fate, behaviour, and implications of ZnO nanoparticles in a simulated wastewater treatment plant. *Water SA* **2016**, *42*, 72–81. [CrossRef]
45. Khan, A.U.H.; Liu, Y.; Naidu, R.; Fang, C.; Dharmarajan, R.; Shon, H. Interactions between zinc oxide nanoparticles and hexabromocyclododecane in simulated waters. *Environ. Technol. Innov.* **2021**, *24*, 102078. [CrossRef]
46. Khan, R.; Inam, M.A.; Zam, S.Z.; Park, D.R.; Yeom, I.T. Assessment of Key Environmental Factors Influencing the Sedimentation and Aggregation Behavior of Zinc Oxide Nanoparticles in Aquatic Environment. *Water* **2018**, *10*, 660. [CrossRef]
47. Sang, M.; Shin, J.; Kim, K.; Yu, K.J. Electronic and Thermal Properties of Graphene and Recent Advances in Graphene Based Electronics Applications. *Nanomaterials* **2019**, *9*, 374. [CrossRef]
48. Akbar, F.; Kolahdouz, M.; Larimian, S.; Radfar, B.; Radamson, H.H. Graphene synthesis, characterization and its applications in nanophotonics, nanoelectronics, and nanosensing. *J. Mater. Sci. Mater. Electron.* **2015**, *26*, 4347–4379. [CrossRef]
49. Vidu, R.; Matei, E.; Predescu, A.M.; Alhalaili, B.; Pantilimon, C.; Tarcea, C.; Predescu, C. Removal of Heavy Metals from Wastewaters: A Challenge from Current Treatment Methods to Nanotechnology Applications. *Toxics* **2020**, *8*, 101. [CrossRef] [PubMed]
50. Kong, Q.; Shi, X.; Ma, W.; Zhang, F.; Yu, T.; Zhao, F.; Zhao, D.; Wei, C. Strategies to improve the adsorption properties of graphene-based adsorbent towards heavy metal ions and their compound pollutants: A review. *J. Hazard. Mater.* **2021**, *415*, 125690. [CrossRef]
51. Kavitha, C. A review on reduced Graphene oxide hybrid nano composites and their prominent applications. *Mater. Today Proc.* **2022**, *49*, 811–816. [CrossRef]
52. Khedekar, V.V.; Zaeem, S.M.; Das, S. Graphene-metal oxide nanocomposites for supercapacitors: A perspective review. *Adv. Mater. Lett.* **2018**, *9*, 2–19. [CrossRef]
53. Sontakke, A.D.; Tiwari, S.; Purkait, M.K. A comprehensive review on graphene oxide-based nanocarriers: Synthesis, functionalization and biomedical applications. *FlatChem* **2023**, *38*, 100484. [CrossRef]
54. Dar, R.A.; Naikoo, G.A.; Srivastava, A.K.; Hassan, I.U.; Karna, S.P.; Giri, L.; Shaikh, A.M.H.; Rezakazemi, M.; Ahmed, W. Performance of graphene-zinc oxide nanocomposite coated-glassy carbon electrode in the sensitive determination of para-nitrophenol. *Sci. Rep.* **2022**, *12*, 117. [CrossRef]
55. Saranya, M.; Ramachandran, R.; Wang, F. Graphene-zinc oxide (G-ZnO) nanocomposite for electrochemical supercapacitor applications. *J. Sci. Adv. Mater. Devices* **2016**, *1*, 454–460. [CrossRef]
56. Dash, B.S.; Jose, G.; Lu, Y.J.; Chen, J.P. Functionalized Reduced Graphene Oxide as a Versatile Tool for Cancer Therapy. *Int. J. Mol. Sci.* **2021**, *22*, 2989. [CrossRef] [PubMed]
57. Afzal, H.; Ikram, M.; Ali, S.; Shahzadi, A.; Aqeel, M.; Haider, A.; Imran, M.; Ali, S. Enhanced drug efficiency of doped ZnO–GO (graphene oxide) nanocomposites, a new gateway in drug delivery systems (DDSs). *Mater. Res. Express* **2020**, *7*, 015405. [CrossRef]
58. Nagaraj, E.; Shanmugam, P.; Karuppannan, K.; Chinnasamy, T.; Venugopal, S. The biosynthesis of a graphene oxide-based zinc oxide nanocomposite using Dalbergia latifolia leaf extract and its biological applications. *New J. Chem.* **2020**, *44*, 2166–2179. [CrossRef]
59. Toporovska, L.; Turko, B.; Savchak, M.; Seyedi, M.; Luzinov, I.; Kostruba, A.; Kapustianyk, V.; Vaskiv, A. Zinc oxide: Reduced graphene oxide nanocomposite film for heterogeneous photocatalysis. *Opt. Quantum Electron.* **2020**, *52*, 21. [CrossRef]
60. Zhang, L.; Li, N.; Jiu, H.; Qi, G.; Huang, Y. ZnO-reduced graphene oxide nanocomposites as efficient photocatalysts for photocatalytic reduction of CO_2. *Ceram. Int.* **2015**, *41*, 6256–6262. [CrossRef]

61. Ensafi Avval, M.; Moghadam, P.N.; Baradarani, M.M. Synthesis of a new nanocomposite based-on graphene-oxide for selective removal of Pb^{2+} ions from aqueous solutions. *Polym. Compos.* **2019**, *40*, 730–737. [CrossRef]
62. Sahoo, S.K.; Hota, G. Functionalization of graphene oxide with metal oxide nanomaterials: Synthesis and applications for the removal of inorganic, toxic, environmental pollutants from water. In *Handbook of Functionalized Nanomaterials for Industrial Applications*; Elsevier: Amsterdam, The Netherlands, 2020; pp. 299–326.
63. Ranjith, K.S.; Manivel, P.; Rajendrakumar, R.T.; Uyar, T. Multifunctional ZnO nanorod-reduced graphene oxide hybrids nanocomposites for effective water remediation: Effective sunlight driven degradation of organic dyes and rapid heavy metal adsorption. *Chem. Eng. J.* **2017**, *325*, 588–600. [CrossRef]
64. Ali, I.; Peng, C.; Naz, I.; Amjed, M.A. Water Purification Using Magnetic Nanomaterials: An Overview. In *Nanotechnology in the Life Sciences*; Springer: Cham, Switzerland, 2019; pp. 161–179.
65. Abd-Elhamid, A.I.; Elgoud, E.M.A.; Aly, H.F. Alginate modified graphene oxide for rapid and effective sorption of some heavy metal ions from an aqueous solution. *Cellulose* **2022**, *29*, 6231–6245. [CrossRef]
66. Bharadwaj, P.; Kiran, G.R.; Acharyya, S.G. Remarkable performance of GO/ZnO nanocomposites under optimized parameters for remediation of Cd (II) from water. *Appl. Surf. Sci.* **2023**, *626*, 157238. [CrossRef]
67. Joshi, N.C.; Gururani, P. Advances of graphene oxide based nanocomposite materials in the treatment of wastewater containing heavy metal ions and dyes. *Curr. Res. Green Sustain. Chem.* **2022**, *5*, 100306. [CrossRef]
68. Maqbool, A.; Shahid, A.; Jahan, Z.; Bilal Khan Niazi, M.; Ali Inam, M.; Tawfeek, A.M.; M Kamel, E.; Saeed Akhtar, M. Development of ZnO-GO-NiO membrane for removal of lead and cadmium heavy metal ions from wastewater. *Chemosphere* **2023**, *338*, 139622. [CrossRef] [PubMed]
69. El Maguana, Y.; Elhadiri, N.; Benchanaa, M.; Chikri, R. Activated Carbon for Dyes Removal: Modeling and Understanding the Adsorption Process. *J. Chem.* **2020**, *2020*, 1. [CrossRef]
70. Ramadan, R.; Abdel-Aal, S.K. Facile synthesis of nanostructured ZnO–rGO based graphene and its application in wastewater treatment. *J. Mater. Sci. Mater. Electron.* **2021**, *32*, 19667–19675. [CrossRef]
71. Ghozatloo, A.; Enayatollahi, A. Enhancing the effect of zinc oxide on the absorption of heavy metals from wastewater by using silica in graphene bed. *Anal. Methods Environ. Chem. J.* **2019**, *2*, 27–38. [CrossRef]
72. Nik-Abdul-Ghani; Jami; Alam The role of nanoadsorbents and nanocomposite adsorbents in the removal of heavy metals from wastewater: A review and prospect. *Pollution* **2021**, *7*, 153–179. [CrossRef]
73. Joshi, N.C.; Rawat, B.S.; Kumar, P.; Kumar, N.; Upadhyay, S.; Chetana, S.; Gururani, P.; Kimothi, S. Sustainable synthetic approach and applications of ZnO/r-GO in the adsorption of toxic Pb^{2+} and Cr^{6+} ions. *Inorg. Chem. Commun.* **2022**, *145*, 110040. [CrossRef]
74. Naseem, T.; Zain-ul-Abdin; Waseem, M.; Hafeez, M.; Din, S.U.; Haq, S.; Mahfoz-ur-Rehman. Reduced Graphene Oxide/Zinc Oxide Nanocomposite: From Synthesis to its Application for Wastewater Purification and Antibacterial Activity. *J. Inorg. Organomet. Polym. Mater.* **2020**, *30*, 3907–3919. [CrossRef]
75. Zhao, X.; Hu, B.; Ye, J.; Jia, Q. Preparation, Characterization, and Application of Graphene–Zinc Oxide Composites (G–ZnO) for the Adsorption of Cu(II), Pb(II), and Cr(III). *J. Chem. Eng. Data* **2013**, *58*, 2395–2401. [CrossRef]
76. Ahmed, M.A.; Ahmed, M.A.; Mohamed, A.A. Facile adsorptive removal of dyes and heavy metals from wastewaters using magnetic nanocomposite of zinc ferrite@reduced graphene oxide. *Inorg. Chem. Commun.* **2022**, *144*, 109912. [CrossRef]
77. Hosseinkhani, O.; Hamzehlouy, A.; Dan, S.; Sanchouli, N.; Tavakkoli, M.; Hashemipour, H. Graphene oxide/ZnO nanocomposites for efficient removal of heavy metal and organic contaminants from water. *Arab. J. Chem.* **2023**, *16*, 105176. [CrossRef]
78. Guo, T.; Bulin, C.; Li, B.; Zhao, Z.; Yu, H.; Sun, H.; Ge, X.; Xing, R.; Zhang, B. Efficient removal of aqueous Pb(II) using partially reduced graphene oxide-Fe_3O_4. *Adsorpt. Sci. Technol.* **2018**, *36*, 1031–1048. [CrossRef]
79. Kumari, V.; Kaushal, S.; Singh, P.P. Green synthesis of a CuO/rGO nanocomposite using a Terminalia arjuna bark extract and its catalytic activity for the purification of water. *Mater. Adv.* **2022**, *3*, 2170–2184. [CrossRef]
80. Al-Qahtani, K.M.; Ali, M.H.H.; Al-Afify, A.G. Synthesis and use of TiO_2@rGo nanocomposites in photocatalytic removal of chromium and lead ions from wastewater. *J. Elem.* **2020**, *25*, 315–322. [CrossRef]
81. Joshi, N.C.; Rawat, B.S.; Semwal, P.; Kumar, N. Effective removal of highly toxic Pb^{2+} and Cd^{2+} ions using reduced graphene oxide, polythiophene, and silica-based nanocomposite. *J. Dispers. Sci. Technol.* **2022**, *2022*, 58–67. [CrossRef]
82. Mashkoor, F.; Shoeb, M.; Mashkoor, R.; Anwer, A.H.; Zhu, S.; Jeong, H.; Baek, S.S.; Jung, J.; Jeong, C. Synergistic effects of tungstate trioxide hemihydrate decorated reduced graphene oxide for the adsorption of heavy metals and dyes and postliminary application in supercapacitor device. *J. Clean. Prod.* **2023**, *418*, 138067. [CrossRef]
83. Eftekhari, M.; Akrami, M.; Gheibi, M.; Azizi-Toupkanloo, H.; Fathollahi-Fard, A.M.; Tian, G. Cadmium and copper heavy metal treatment from water resources by high-performance folic acid-graphene oxide nanocomposite adsorbent and evaluation of adsorptive mechanism using computational intelligence, isotherm, kinetic, and thermodynamic analyses. *Environ. Sci. Pollut. Res.* **2020**, *27*, 43999–44021. [CrossRef]
84. Nandi, D.; Basu, T.; Debnath, S.; Ghosh, A.K.; De, A.; Ghosh, U.C. Mechanistic insight for the sorption of Cd(II) and Cu(II) from aqueous solution on magnetic mn-doped Fe(III) oxide nanoparticle implanted graphene. *J. Chem. Eng. Data* **2013**, *58*, 2809–2818. [CrossRef]
85. Davis, K.; Yarbrough, R.; Froeschle, M.; White, J.; Rathnayake, H. Band gap engineered zinc oxide nanostructures via a sol–gel synthesis of solvent driven shape-controlled crystal growth. *RSC Adv.* **2019**, *9*, 14638–14648. [CrossRef]

86. Zhang, C.; Tu, Q.; Francis, L.F.; Kortshagen, U.R. Band Gap Tuning of Films of Undoped ZnO Nanocrystals by Removal of Surface Groups. *Nanomaterials* **2022**, *12*, 565. [CrossRef] [PubMed]
87. Rabchinskii, M.K.; Shnitov, V.V.; Dideikin, A.T.; Aleksenskii, A.E.; Vul, S.P.; Baidakova, M.V.; Pronin, I.I.; Kirilenko, D.A.; Brunkov, P.N.; Weise, J.; et al. Nanoscale perforation of graphene oxide during photoreduction process in the argon atmosphere. *J. Phys. Chem. C* **2016**, *120*, 28261–28269. [CrossRef]
88. Faniyi, I.O.; Fasakin, O.; Olofinjana, B.; Adekunle, A.S.; Oluwasusi, T.V.; Eleruja, M.A.; Ajayi, E.O.B. The comparative analyses of reduced graphene oxide (RGO) prepared via green, mild and chemical approaches. *SN Appl. Sci.* **2019**, *1*, 1181. [CrossRef]
89. Alamdari, S.; Ghamsari, M.S.; Lee, C.; Han, W.; Park, H.H.; Tafreshi, M.J.; Afarideh, H.; Ara, M.H.M. Preparation and Characterization of Zinc Oxide Nanoparticles Using Leaf Extract of Sambucus ebulus. *Appl. Sci.* **2020**, *10*, 3620. [CrossRef]
90. Balogun, S.W.; James, O.O.; Sanusi, Y.K.; Olayinka, O.H. Green synthesis and characterization of zinc oxide nanoparticles using bashful (Mimosa pudica), leaf extract: A precursor for organic electronics applications. *SN Appl. Sci.* **2020**, *2*, 504. [CrossRef]
91. Ramesh, P.; Saravanan, K.; Manogar, P.; Johnson, J.; Vinoth, E.; Mayakannan, M. Green synthesis and characterization of biocompatible zinc oxide nanoparticles and evaluation of its antibacterial potential. *Sens. Bio-Sens. Res.* **2021**, *31*, 100399. [CrossRef]
92. Yasin, A.S.; Yousef Mohamed, A.; Kim, D.H.; Luu Luyen Doan, T.; Chougule, S.S.; Jung, N.; Nam, S.; Lee, K. Design of zinc oxide nanoparticles and graphene hydrogel co-incorporated activated carbon for efficient capacitive deionization. *Sep. Purif. Technol.* **2021**, *277*, 119428. [CrossRef]
93. Bhuyan, B.; Paul, B.; Purkayastha, D.D.; Dhar, S.S.; Behera, S. Facile synthesis and characterization of zinc oxide nanoparticles and studies of their catalytic activity towards ultrasound-assisted degradation of metronidazole. *Mater. Lett.* **2016**, *168*, 158–162. [CrossRef]
94. Pitiphattharabun, S.; Auewattanapun, K.; Htet, T.L.; Thu, M.M.; Panomsuwan, G.; Techapiesancharoenkij, R.; Ohta, J.; Jongprateep, O. Reduced graphene oxide/zinc oxide composite as an electrochemical sensor for acetylcholine detection. *Sci. Rep.* **2024**, *14*, 14224. [CrossRef] [PubMed]
95. Jayachandiran, J.; Yesuraj, J.; Arivanandhan, M.; Raja, A.; Suthanthiraraj, S.A.; Jayavel, R.; Nedumaran, D. Synthesis and Electrochemical Studies of rGO/ZnO Nanocomposite for Supercapacitor Application. *J. Inorg. Organomet. Polym. Mater.* **2018**, *28*, 2046–2055. [CrossRef]
96. Chitradevi, T.; Jestin Lenus, A.; Victor Jaya, N. Structure, morphology and luminescence properties of sol-gel method synthesized pure and Ag-doped ZnO nanoparticles. *Mater. Res. Express* **2019**, *7*, 015011. [CrossRef]
97. Drmosh, Q.A.; Yamani, Z.H.; Hendi, A.H.; Gondal, M.A.; Moqbel, R.A.; Saleh, T.A.; Khan, M.Y. A novel approach to fabricating a ternary rGO/ZnO/Pt system for high-performance hydrogen sensor at low operating temperatures. *Appl. Surf. Sci.* **2019**, *464*, 616–626. [CrossRef]
98. Rodwihok, C.; Wongratanaphisan, D.; Ngo, Y.L.T.; Khandelwal, M.; Hur, S.H.; Chung, J.S. Effect of GO Additive in ZnO/rGO Nanocomposites with Enhanced Photosensitivity and Photocatalytic Activity. *Nanomaterials* **2019**, *9*, 1441. [CrossRef]
99. Sharma, V.; Jain, Y.; Kumari, M.; Gupta, R.; Sharma, S.K.; Sachdev, K. Synthesis and Characterization of Graphene Oxide (GO) and Reduced Graphene Oxide (rGO) for Gas Sensing Application. *Macromol. Symp.* **2017**, *376*, 1700006. [CrossRef]
100. Surekha, G.; Krishnaiah, K.V.; Ravi, N.; Padma Suvarna, R. FTIR, Raman and XRD analysis of graphene oxide films prepared by modified Hummers method. *J. Phys. Conf. Ser.* **2020**, *1495*, 012012. [CrossRef]
101. Korepanov, V.I.; Chan, S.Y.; Hsu, H.C.; Hamaguchi, H.O. Phonon confinement and size effect in Raman spectra of ZnO nanoparticles. *Heliyon* **2019**, *5*, e01222. [CrossRef]
102. Thakur, S.; Mandal, S.K. Precursor-and Time-Dependent Morphological Evolution of ZnO Nanostructures for Comparative Photocatalytic Activity and Adsorption Dynamics with Methylene Blue Dye. *ACS Omega* **2020**, *5*, 16670–16680. [CrossRef]
103. Xu, T.; Zhang, L.; Cheng, H.; Zhu, Y. Significantly enhanced photocatalytic performance of ZnO via graphene hybridization and the mechanism study. *Appl. Catal. B Environ.* **2011**, *101*, 382–387. [CrossRef]
104. Cobianu, C.; Cobianu, C.; Dumbravescu, N.; Serban, B.C.; Buiu, O.; Romanitan, C.; Comanescu, F.; Danila, M.; Marinescu, R.; Avramescu, V.; et al. Sonochemically synthetized ZnO-graphene nanohybrids and its characterization. *Rev. Adv. Mater. Sci.* **2020**, *59*, 176–187. [CrossRef]
105. Kumar, A.; Sadanandhan, A.M.; Jain, S.L. Silver doped reduced graphene oxide as a promising plasmonic photocatalyst for oxidative coupling of benzylamines under visible light irradiation. *New J. Chem.* **2019**, *43*, 9116–9122. [CrossRef]
106. Kalpana, V.N.; Kataru, B.A.S.; Sravani, N.; Vigneshwari, T.; Panneerselvam, A.; Devi Rajeswari, V. Biosynthesis of zinc oxide nanoparticles using culture filtrates of Aspergillus niger: Antimicrobial textiles and dye degradation studies. *OpenNano* **2018**, *3*, 48–55. [CrossRef]
107. Ahmad, Z.; UllahKha, F.; Mahmood, S.; Mahmood, T.; Shamim, A. Different Approaches for the Synthesis of Zinc Oxide Nanoparticles. *Open J. Chem.* **2018**, *1*, 19–25. [CrossRef]
108. Kiranakumar, H.V.; Naveen, C.S.; Thejas, R.; Prasanna, G.D.; Nagaraju, G.; Murugendrappa, M. V An impact of RGO on the ZnO nanoparticles: Structural, morphological, electrical, and gas sensing properties. *Sens. Technol.* **2024**, *2*, 2310479. [CrossRef]
109. Nikolaychuk, P.A. The revised potential—pH diagram for Pb—H_2O system. *Ovidius Univ. Ann. Chem.* **2018**, *29*, 55–67. [CrossRef]
110. Alghamdi, A.A.; Al-Odayni, A.B.; Saeed, W.S.; Al-Kahtani, A.; Alharthi, F.A.; Aouak, T. Efficient Adsorption of Lead (II) from Aqueous Phase Solutions Using Polypyrrole-Based Activated Carbon. *Materials* **2019**, *12*, 2020. [CrossRef]

111. Zaimee, M.Z.A.; Sarjadi, M.S.; Rahman, M.L. Heavy Metals Removal from Water by Efficient Adsorbents. *Water* **2021**, *13*, 2659. [CrossRef]
112. Akpomie, K.G.; Conradie, J.; Adegoke, K.A.; Oyedotun, K.O.; Ighalo, J.O.; Amaku, J.F.; Olisah, C.; Adeola, A.O.; Iwuozor, K.O. Adsorption mechanism and modeling of radionuclides and heavy metals onto ZnO nanoparticles: A review. *Appl. Water Sci.* **2022**, *13*, 20. [CrossRef]
113. Moosavi, S.; Lai, C.W.; Gan, S.; Zamiri, G.; Akbarzadeh Pivehzhani, O.; Johan, M.R. Application of efficient magnetic particles and activated carbon for dye removal from wastewater. *ACS Omega* **2020**, *5*, 20684–20697. [CrossRef]
114. Prabhu, S.M.; Rane, N.R.; Li, X.; Otari, S.V.; Girawale, S.D.; Palake, A.R.; Kodam, K.M.; Park, Y.-K.; Ha, Y.-H.; Yadav, K.K.; et al. Magnetic nanostructured adsorbents for water treatment: Structure-property relationships, chemistry of interactions, and lab-to-industry integration. *Chem. Eng. J.* **2023**, *468*, 143474. [CrossRef]
115. Liao, W.; Zhou, X.; Cai, N.; Chen, Z.; Yang, H.; Zhang, S.; Zhang, X.; Chen, H. Simultaneous removal of cadmium, lead, chromate by biochar modified with layered double hydroxide with sulfide intercalation. *Bioresour. Technol.* **2022**, *360*, 127630. [CrossRef] [PubMed]
116. Gupta, A.; Sharma, V.; Sharma, K.; Kumar, V.; Choudhary, S.; Mankotia, P.; Kumar, B.; Mishra, H.; Moulick, A.; Ekielski, A.; et al. A Review of Adsorbents for Heavy Metal Decontamination: Growing Approach to Wastewater Treatment. *Materials* **2021**, *14*, 4702. [CrossRef] [PubMed]
117. Verma, M.; Lee, I.; Hong, Y.; Kumar, V.; Kim, H. Multifunctional β-Cyclodextrin-EDTA-Chitosan polymer adsorbent synthesis for simultaneous removal of heavy metals and organic dyes from wastewater. *Environ. Pollut.* **2022**, *292*, 118447. [CrossRef]
118. Ahmad, S.Z.N.; Salleh, W.N.W.; Yusof, N.; Mohd Yusop, M.Z.; Hamdan, R.; Awang, N.A.; Ismail, N.H.; Rosman, N.; Sazali, N.; Ismail, A.F. Pb(II) removal and its adsorption from aqueous solution using zinc oxide/graphene oxide composite. *Chem. Eng. Commun.* **2020**, *208*, 646–660. [CrossRef]
119. Huang, H.; Wang, Y.; Zhang, Y.; Niu, Z.; Li, X. Amino-functionalized graphene oxide for Cr(VI), Cu(II), Pb(II) and Cd(II) removal from industrial wastewater. *Open Chem.* **2020**, *18*, 97–107. [CrossRef]
120. Cherono, F.; Mburu, N.; Kakoi, B. Adsorption of lead, copper and zinc in a multi-metal aqueous solution by waste rubber tires for the design of single batch adsorber. *Heliyon* **2021**, *7*, e08254. [CrossRef]